Challenge Journal of STRUCTURAL MECHANICS

Vol.5 No.1 (2019)

Mindlin's theory buckling building codes dynamic analysis dynamic response earthquake elastic foundation finite element analysis finite element method nonlinear analysis operational modal analysis optimization prestressing pushover analysis reinforced concrete seismic analysis seismic design seismic isolation soil-structure interaction temperature effects thick plate wind

ISSN 2149-8024

TULPAR ACADEMIC PUBLISHING

Challenge Journal of Structural Mechanics

E-mail: *cjsmec@challengejournal.com*

Web page: *cjsmec.challengejournal.com*

TULPAR Academic Publishing
www.tulparpublishing.com

Challenge Journal of Structural Mechanics

CONTENTS

Research Articles

TULPAR ACADEMIC PUBLISHING

Challenge Journal of Structural Mechanics

Research Article

Estimation of capacity of eccentrically loaded single angle struts with decision trees

Saha Dauji

Bhabha Atomic Research Centre, Homi Bhabha National Institute, Anushaktinagar, Mumbai 400094, India

ABSTRACT

Single angle struts are used as compression members for many structures including roof trusses and transmission towers. The exact analysis and design of such members is challenging due to various uncertainties such as the end fixity or eccentricity of the applied loads. The design standards provide guidelines that have been found inaccurate towards the conservative side. Artificial Neural Networks (ANN) have been observed to perform better than the design standards, when trained with experimental data and this has been reported literature. However, practical implementation of ANN poses problem as the trained network as well as the knowhow regarding the application should be accessible to practitioners. In another data-driven tool, the Decision Trees (DT), the practical application is easier as decision based rules are generated, which are readily comprehended and implemented by designers. Hence, in this paper, DT was explored for the evaluation of capacity of eccentrically loaded single angle struts and was found to be robust and yielded comparable accuracy as ANN, and better than design code (AISC). This has enormous potential for easy and straightforward implementation by practicing engineers through the logic based decision rules, which would be easily programmable on computer. For this application, use of dimensionless ratios as inputs for the development of DT was found to yield better results when compared to the approach of using the original variables as inputs.

ARTICLE INFO

Article history:
Received 3 October 2018
Revised 28 December 2018
Accepted 14 January 2019

Keywords:
Eccentric loading
Single angle
Strut
Compressive capacity
Decision tree

1. Introduction

In construction of steel structures, use of single angle struts is quite common and often their connections lead to eccentricity of loading in both the axes. This had been attributed to factors like eccentricity of applied load, mismatch of the axis of the frame and the angle, and some degree of fixity occurring at the connections (Sakla, 2004). The complexity of behaviour of these struts arising out of the factors mentioned above, make accurate estimation of their load carrying capacity quite challenging. The possible modes of failure might include compression, flexural buckling, and torsional-flexural buckling. The exact analysis as enumerated in design codes (AISC, 2000) becomes difficult due to all these complexities and uncertainties. The design recommendations (Fisher, 2000; Page, 2005) for these members which were based on analytical models and some experimental results had been reported in literature to be on the conservative side (Sakla, 2004; Liu and Hui, 2008).

There were various experimental investigations reported in literature wherein compressive capacity of single angle struts were determined for different eccentricities and slenderness ratios. Analytical, empirical and numerical investigations had been carried out by researchers for improving the understanding of the behaviour of single angle struts and estimation of their ultimate compressive capacity under eccentricities. Wakabayashi and Nonaka (1965) compared the experimental results from 57 tests with the buckling theories. Woolcock and Kitipornchai (1986) presented a design approach based on experimental results for single angle struts connected with a single leg. Elgaaly et al. (1991) evaluated AISC design recommendations with test results of single angle struts with low slenderness ratios.

* *Corresponding author*. Tel.: +91-222-559-7985 ; E-mail address: acad.dauji@gmail.com (S. Dauji)
ISSN: 2149-8024 / DOI: https://doi.org/10.20528/cjsmec.2019.01.001

Bathon et al. (1993) examined the test results of ultimate load capacity of single angle struts along with the AISC design guidelines. Adluri and Madugela (1996) presented the results from tests on single angle sections for concentric compressive loads failing in flexural buckling. Rao et al. (2003) explored the design issues of such struts with numerical investigation accounting for the material and geometric nonlinearities and proposed a design approach. Sakla (2004) explored the neural network approach for estimation of the compressive capacity on the basis of published experimental data. Liu and Hui (2008) compared the experimental results with the AISC design and concluded that the AISC gave conservative results, especially for struts subjected to eccentricity about the major principal axis. In a subsequent study, Liu and Hui (2010) confirmed the earlier finding with numerical modelling based on finite element techniques.

In their study, Liu and Chantel (2011) examined the responses of single angle struts for eccentric compressive loads and concluded that the effect of eccentricity on the ultimate load decreased with increasing slenderness ratio. Bashar and Amanat (2014) investigated the ultimate axial capacity of eccentrically loaded angles with numerical technique accounting for the geometric and material nonlinearities. Barszcz (2014) developed analytical formulation for simulating the force-deflection behaviour of single angle struts and validated the model with experimental results.

For the practicing designers, simulating the behaviour of single angle struts and the end conditions in the actual frame or truss was a big challenge. Most of the design codes have guidelines that were empirical in nature, with their own limitations. The numerical approach with intricate finite element model of each strut for evaluation of the stresses and deflections was very demanding on resources to be useful for practical design. Simpler methods of estimation of the ultimate compressive load capacity of single angle struts had been proposed based on artificial neural network (ANN) by Sakla (2004). However, implementation of ANN for practical design poses challenge that is yet to be resolved.

Decision Tree (DT), concurrently known as Model Tree (MT) or Regression Tree (RT), had been utilized in some civil engineering applications including hydrology, geotechnical applications, and concrete technology in the past. Garg et al. (2008) discussed an application of Model Tree (MT or DT) for prediction of currents (in future: output) in tide-dominated areas like gulfs and creeks from past current records (inputs) and concluded that the MT was faster by orders of magnitude compared to ANN and Genetic Programming (GP) models while producing comparable forecasts. Tiraki (2008) employed multivariate statistics, ANN and regression tree (or DT) for predicting uniaxial compressive strength (output) and static modulus of elasticity (output) from other rock properties (inputs) and concluded that the DT were best for development of such predictive models. Kim and Pachepsky (2010) used regression tree (or DT) in conjunction with ANN for reconstructing the missing data (output) in daily precipitation records from adjacent precipitation data (inputs).

Using experimental data from literature, Ayaz et al. (2015) employed DT for predicting the compressive strength (output) and ultrasonic pulse velocity (output) for HPC from ingredients (inputs) with 97% and 87% success respectively. Behnood et al. (2015) predicted the modulus of elasticity (output) of recycled aggregate concrete from the ingredients (inputs) using DT with 80% accuracy. Gharaei-Manesh et al. (2016) employed ANN and DT for estimating the snow depth (output) from terrain parameters (inputs) in the Sakhvid Basin in Iran and concluded that DT had superiority over ANN for that application. Dauji (2016) utilized the DT for prediction of compressive strength of concrete (output) from its ingredients (inputs) and concluded that performance of DT was superior to that of ANN reported in literature. Furthermore, it was noted that for certain applications, DT had been reported to give faster and superior performance as compared to other data driven tools like ANN.

In this article it is proposed to explore application of another data-driven tool, the DT for this particular application and compare its accuracy with that of the ANN. ANN had been reported to be quite accurate in estimation of compressive capacity of eccentrically loaded single angle struts. If DT model has similar accuracy as ANN, it would hold comparative advantage over ANN in implementation by practising designers, as it gives a set of rules for estimation of the target variable. In this paper, the data-driven tool Decision Tree (DT) was employed for predicting the capacity of eccentrically loaded single angles under compressive loads.

2. Data and Methodology

This study was based on the published experimental data obtained from literature (Wakabayashi and Nonaka, 1965; Ishida, 1968; Mueller and Erzurumlu, 1983; Bathon et al., 1993; Adluri and Madugula, 1996; Liu and Hui, 2008). The accumulated data was filtered so as to arrive at a collection of ultimate compressive strength of single angle struts under various eccentricities, with the end conditions being hinged at both ends. The resulting database contained 153 sets of data which were then used for development and evaluation of the DT. The data was taken from the experimental studies reported by: (a) Wakabayashi and Nonaka (1965); (b) Ishida (1968) (c) Mueller and Erzurumlu (1983); (d) Bathon et al. (1993); (e) Adluri and Madugula (1996); (f) Liu and Hui (2008). The test setup and other details of the experiments can be found in aforementioned literature.

The regression tree (RT) alternately known as DT modelling had been described as an exploratory technique based on uncovering structure in data (Clarke, 1991).The popularity of DT is increasing for their simplicity and interpretability, their low computational cost and for the possibility of being graphically represented (Rodriguez-Galiano et al., 2015). In the model space (Fig. 1a), the decision tree process the information from the root node (decision box) to other nodes (decision boxes) or leaves (representing the models or expressions) based on the decision output: 'yes' or 'no' (Fig. 1b). In this way, the model space is progressively subdivided into smaller spaces (Fig. 1a) such that one decision rule prevails in each sub-space. The division of the model space into sub-spaces or domain

splitting is conducted by some algorithm, such as, minimum entropy in sub-domain, or collecting as many samples as possible in the class, or any other. In the popular M5 algorithm of DT, this task is performed by minimizing the standard deviation of the class value reaching a node (Breiman et al., 1984; Quinlan, 1993; Jekabsons G, 2016) and this approach has been adopted in this study.

Accordingly, Fig. 1a shows the domain splitting for two variables (x1 & x2) and the decision tree structure is depicted in Fig. 1b, where the diamonds represent the decision boxes and the rectangles represent the decision rules. The ability of a root node to maximise the reduction in standard deviation is taken as the attribute for its selection. Many possible subdivisions of inputs are explored during the model development and the one that results in the maximum reduction in standard deviation is selected to build linear models within each sub-domain. There are many methods reported in literature, which may be employed for avoiding too many domain splits or large discontinuities between neighbouring models (Witten and Frank, 2000; Rokach and Maimon, 2015; Jekabsons, 2016). For a dataset, the model tree enables subdivision of the data hyperspace and definition of linear models in each sub-domain by the adopted objective function (maximum reduction of standard deviation in M5 algorithm) and the linear decision rules together would describe the relationship between the input and output variables. Further details for the development of decision trees may be obtained from standard text books (Witten and Frank, 2000; Rokach and Maimon, 2015).

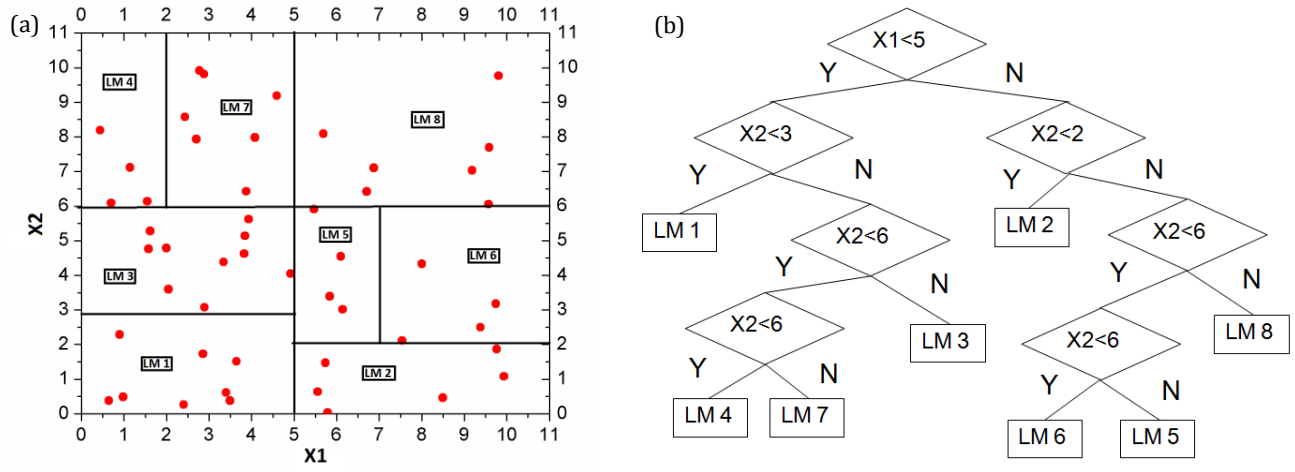

Fig. 1. Decision tree: (a) Domain sub-division; (b) Tree structure.

The DT modelling results in distinct step-wise linear rules to represent the model domain, and hence can be easily implemented by simple programming for new data points within the model domain even without the knowledge of DT development. The modelling by ANN involves establishing the relationship between the input/s (in input layer) and the output/s (in output layer) through the hidden layer/s of neurons, which ensure the desired degree of non-linearity in the relationship. In general, each neuron of a layer is connected with all the neurons in the next layer and the strength of the connection is denoted by weights, which, along with the bias terms of each neuron are ascertained during the process of training process by back propagation of errors. Different algorithms may be applied for the back-propagation of errors such as steepest descent, conjugate gradient, resilient propagation, Levenberg-Marquardt, etc. and for further details regarding development of ANN models, textbooks may be referred (Wasserman, 1993; Bose and Liang, 1993). In case of ANN, the practitioner needs to be acquainted with the concept of modelling in ANN as well as access to the trained ANN & modelling software for implementation of the ANN model for new data points in the model space. When compared with the DT, this is a particular drawback for the ANN models for application by designers. This motivated the present study in which DT is applied for estimation of the capacity of eccentrically loaded single angle struts, for which successful ANN application has already been reported in literature (Sakla, 2004).

For the development of the DT in this study, two approaches were adopted. In the first, the length of the angle leg (b), the thickness of the angle leg (t), the slenderness ratio (l/r), the yield strength of steel (fy), the two eccentricities ($e1$, $e2$) were the input variables (total six) and the ultimate load (P) was the target variable. In the second approach, the dimensionless ratios were used as inputs, namely, ratio of the length to the thickness of the angle leg (b/t), slenderness ratio (l/r), the yield strength of steel (fy), the two relative eccentricities ($e1/b$, $e2/b$) were the input variables (total five) and the ratio of the ultimate load to the yield capacity of the angle (P/Afy) was the target variable. The DT were developed with random assignment of 80% of the data for modelling (123 nos.) and remaining 20% of the data for evaluation of the developed models (30 nos.). Multiple such runs were taken to demonstrate the robustness of the approach. The results of three such runs in either approach are presented and discussed in the subsequent sections.

In this paper, the performance of the DT developed was evaluated with measures like Root Mean Square Relative Error (RMSRE), Mean Absolute Relative Error (MARE), and correlation coefficient (R). RMSRE is a relative error index which is sensitive to the extreme values.

MARE gives an estimate of the relative accuracy of prediction in the absolute scale. The correlation coefficient indicates the degree of linear association between the estimation and the observation and while being sensitive to outliers it is insensitive to proportional or additive differences. The scatter plots of the measured and predicted compressive capacity of struts helped visual evaluation of the accuracy of the models. The ratio of the capacity estimated by the DT and the yield capacity of the angle were evaluated as a measure of the relative accuracy of the DT.

3. Results and Discussion

In the DT-s developed with the actual variables are indicated by 'DTX' and the DT-s developed with ratios as inputs and target are indicated by 'DTRX' in the following sections where 'X' indicates the serial number of the run presented.

The box plots shown in Fig. 2 present the comparison of the various percentiles (mean: small box, median: horizontal in box, 25, 75: extents of box, 1, 99: cross mark, and maximum & minimum: horizontal outside box) for the various random assignment of the data in different runs. It can be noticed that the median is always less than the mean indicating that the tail is longer towards the higher values. For DT cases, it is observed that all the evaluation sets (Eval.) have less spread and standard deviation as compared to the development set (Dev.). However, the range of the first evaluation set is more towards the lower values as compared to the development set. This indicates that the model performance of the first DT case might be affected.

In case of the DTR cases, the spread and the standard deviation are more than, almost equal and less than the respective development sets for the second, third and first cases. This indicates that the model performance of the second DTR case might be affected.

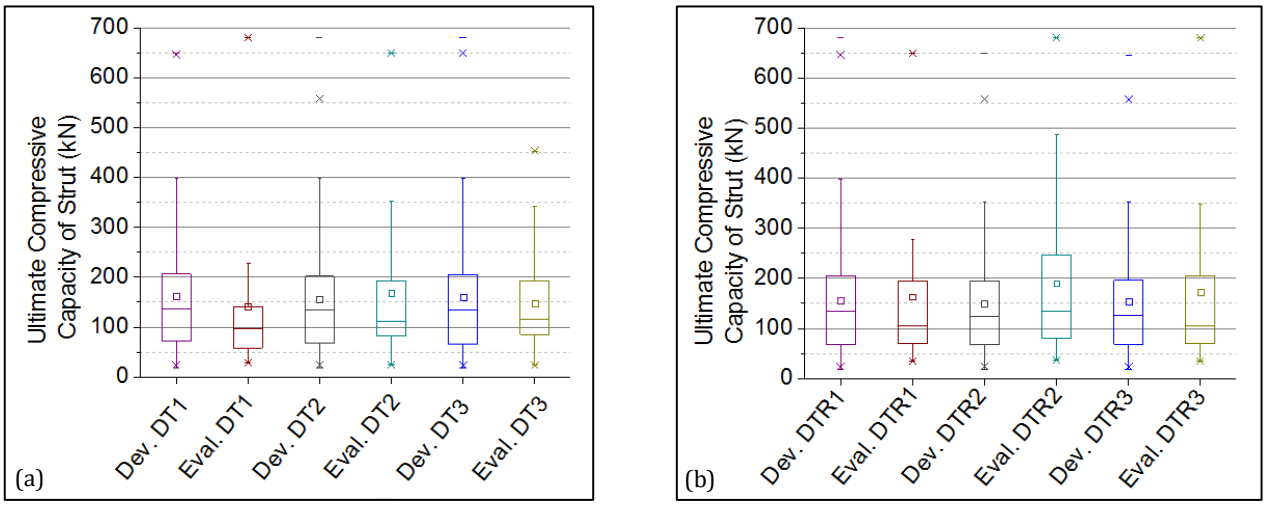

Fig. 2. Data characteristics for the development set (Dev.) and the evaluation (Eval.) set for two approaches: (a) Actual variables; (b) Ratios.

The performance metrics, namely, correlation, RMSRE and MARE, for the different runs are presented in Figs. 3(a-c), respectively. For the DT models, the correlation is around 0.98 while for the DTR models, it rises to 0.99. In general, the RMSRE and the MARE are higher in DT models (between 0.16 – 0.25 and 0.13 – 0.16 respectively) as compared to the DTR models (between 0.14 – 0.16 and 0.10 – 0.13 respectively). This clearly indicates that the use of dimensionless ratios in development of the models have been very beneficial in improving the accuracy of the estimation in the evaluation sets. Among the DT models, the first one is the better and the third DTR model is better one. Overall, the third DTR model appears to be the best amongst all.

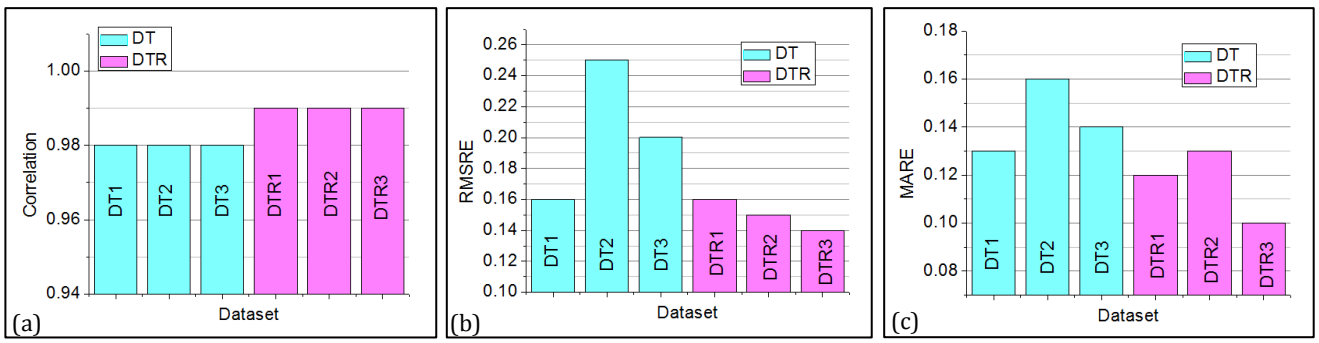

Fig. 3. Performance of the evaluation runs for the two approaches: (a) Correlation; (b) RMRSE; (c) MARE.

The ratio of the estimated ultimate strength and the experimental value has been evaluated for each estimation in the individual runs. The statistics of this relative accuracy is presented as box plots (mean: small box, median: horizontal in box, 25, 75: extents of box, 1, 99: cross mark, and maximum & minimum: horizontal outside box) in Fig. 4. Here it is evident that all the DTR cases are better balanced on either side of unity as compared to the DT cases. The second DTR case has the highest spread and standard deviation among all cases. This could be due to the higher spread and standard deviation of the evaluation set than the development set.

Visual appreciation of the estimation accuracy is possible in the scatter plots shown in Fig. 5 for the DT cases and Fig. 6 for the DTR cases. As indicated earlier, the first DT model appears better and the third DTR model appears better than the rest.

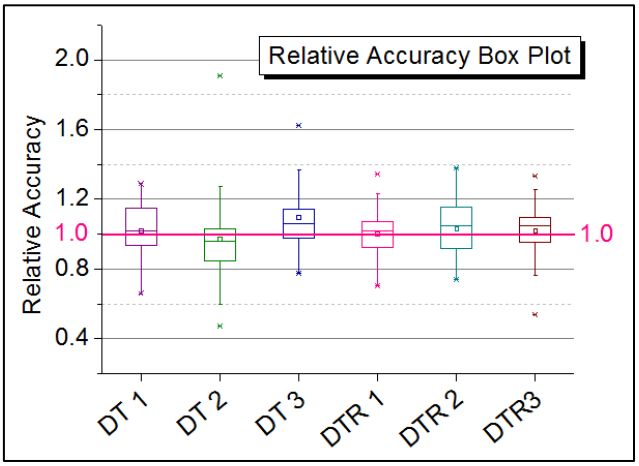

Fig. 4. Data characteristics for the relative accuracy of the different runs in two approaches.

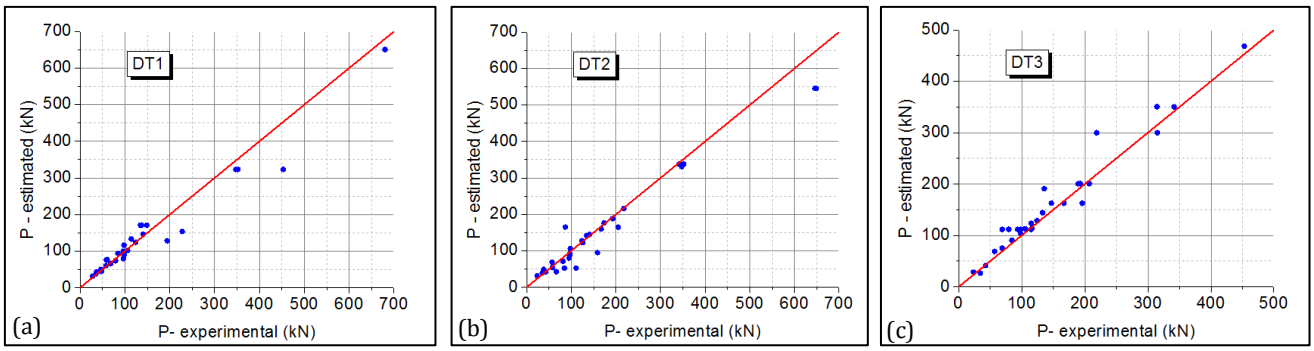

Fig. 5. Scatter plot for the evaluation cases for DT models: (a) Run 1; (b) Run 2; (c) Run 3.

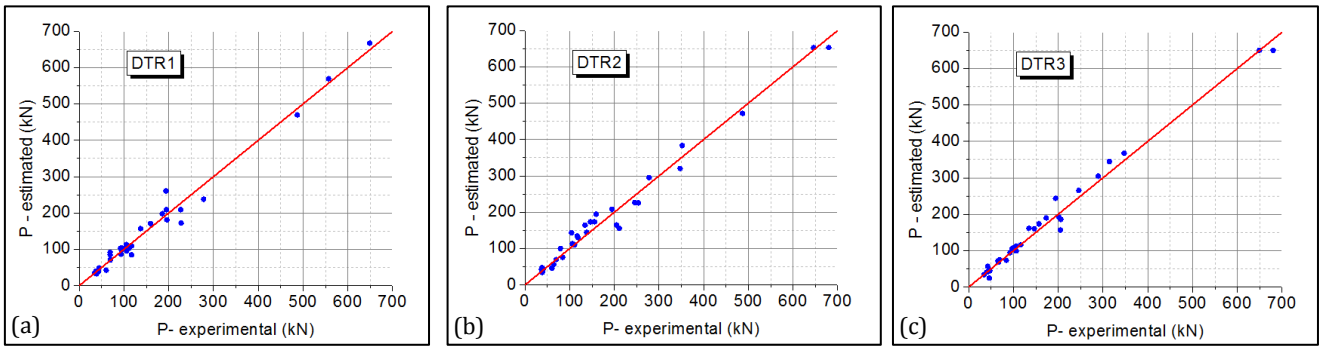

Fig. 6. Scatter plot for the evaluation cases for DTR models: (a) Run 1; (b) Run 2; (c) Run 3.

The data statistics for the experimental and the estimated values of the ultimate compressive capacity in the evaluation sets are shown in the Fig. 7 for both the approaches. Here again it is noted that the best match between the experimental and the estimated happened for the first DT case and the third DTR case. Overall, the statistics of the third DTR matches most closely with those of the experimental evaluation set.

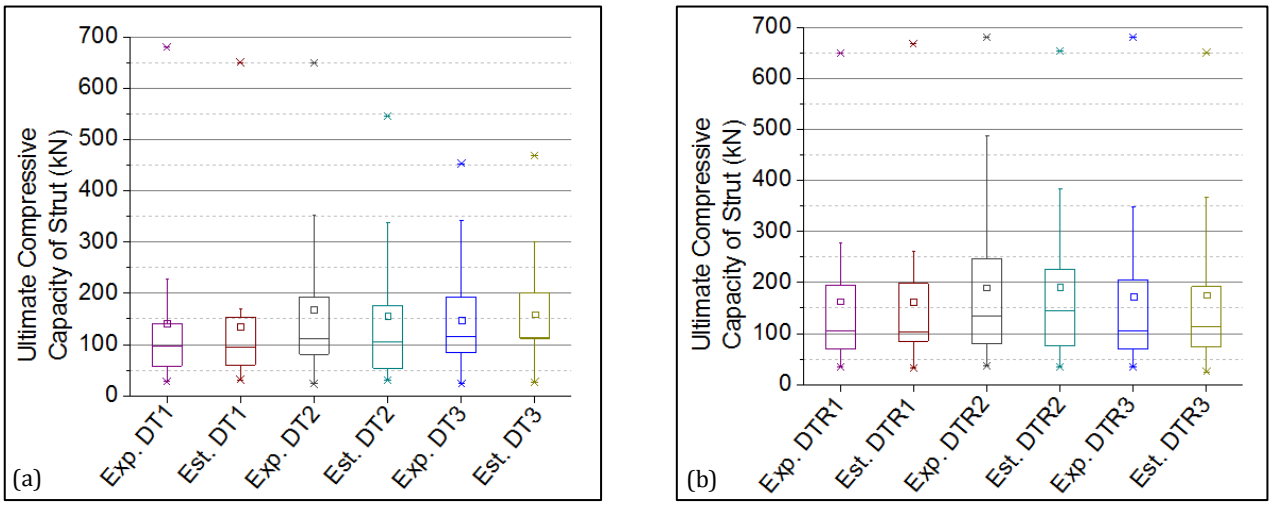

Fig. 7. Data statistics for the experimental and estimated ultimate compressive capacity in evaluation sets (kN): (a) DT models; (b) DTR models.

From the aforementioned discussion, it is concluded that the third DTR model is the best model among all. The structure of the decision tree for the third DTR case is presented in Fig. 8. The rules for the hierarchical splitting are shown at all the intermediate nodes of the decision tree, the numbers in brackets indicate the number of cases passing through the respective nodes. The number of cases passing to the terminal nodes vary between 2 and 11. The explicit models for 'M1' to 'M17' obtained from the DTR3 are presented in Appendix. Read together, the Fig. 8 and the appendix yields a clear-cut evaluation scheme for the ultimate compressive capacity of single angle struts. It may be noted in Table 1 from the performance comparison of DT developed in this study and the ANN (from literature: Sakla, 2004) that the accuracy achieved by the DTR3 is comparable to that reported for ANN and better than the AISC formulations reported in literature (Sakla, 2004).

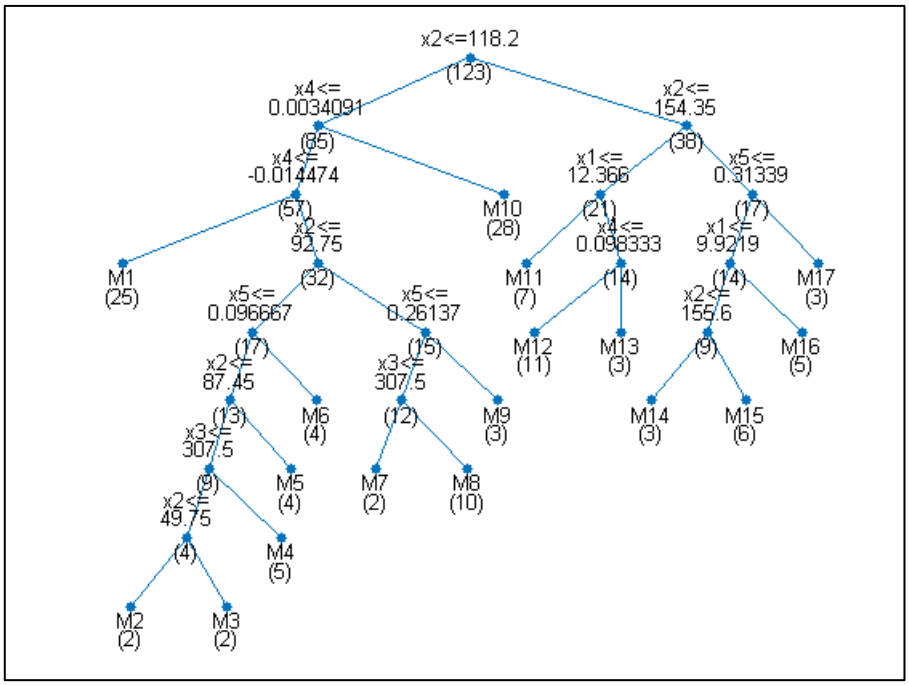

Fig. 8. Structure for the best Decision Tree (DTR3).

Table 1. Comparison of performance of DT (this study) with ANN (Sakla, 2004) and AISC (Sakla, 2004).

Performance Measure	ANN (Sakla, 2004)	AISC (Sakla, 2004)	DT (This study)
Mean Absolute Percentage Error	5.8	12.8	10
Average Ratio of Predicted and Actual Capacity	1.026	0.885	1.02

4. Conclusions

Single angle struts are used in many structures like the roof trusses and transmission towers. The exact analysis and design of single angle struts become difficult owing to uncertainties in evaluation of the eccentricity of the applied load and the fend conditions. In this study, experimental data for ultimate compressive capacity of single angle struts for different eccentricity of loads had been collected from various published articles and using them, attempt had been made to develop an accurate model with DT.

From this study, the following conclusions are drawn:

- The ANN models developed by Sakla (2004) had been demonstrated to be much superior to available AISC formulations. The accuracy of the DT model developed in this study for estimation of the ultimate compressive capacity of single angle struts are comparable to that of ANN models (Sakla, 2004) developed for the same purpose.
- The use of dimensionless ratios in place of actual variables improve the performance of the DT (correlation 0.98, RMSRE 0.16 - 0.25, MARE 0.13 – 0.16 for actual variables; correlation 0.99, RMSRE 0.14 - 0.16, MARE 0.10 – 0.13 for ratio variables).
- For the best DT model developed, correlation of 0.99, RMSRE of 0.14 and MARE of 0.10 could be achieved which indicates very good performance.
- Like other data driven tools, the DT is poor in extrapolation as was seen in the case of DTR2.
- The model DTR3 as presented in Fig. 8 and the appendix may be used by practicing engineers for estimation of the ultimate capacity of single angle struts without any sophisticated analysis like intricate numerical modelling or ANN approach, and thus could be very handy and useful.

Similar performance of the three sets of models in either approach indicates the robustness of the DT approach.

Acknowledgements

The author solemnly acknowledges the various researchers who have published their experimental results that were used in this study.

Appendix

The input variables:
x1: Ratio of the length to the thickness of the angle leg (b/t),
x2 : Slenderness ratio (l/r),
x3 : Yield strength of steel (f_y),
x4, x5 : two relative eccentricities (e_1/b, e_2/b).

The target variable:
Y : ratio of the ultimate load to the yield capacity of the angle (P/Af_y).

Number of rules: 17

Number of original input variables used: 5 (x1, x2, x3, x4, x5)

The Rules:

```
if x2 <= 118.2
 if x4 <= 0.0034091
  if x4 <= -0.014474
   y = 0.66957 -0.0031293*x2 +0.38258*x4 (25)
  else
   if x2 <= 92.75
    if x5 <= 0.096667
     if x2 <= 87.45
      if x3 <= 307.5
       if x2 <= 49.75
        y = 0.91844 (2)
       else
        y = 0.89938 (2)
      else
       y = 0.81902 (5)
     else
      y = 0.70902 (4)
    else
     y = 0.60708 -0.0015359*x2 (4)
   else
    if x5 <= 0.26137
     if x3 <= 307.5
      y = 0.64014 (2)
     else
      y = 0.47126 (10)
    else
     y = 0.15279 (3)
 else
  y = 0.92135 -0.031689*x1 -0.0016546*x2 -0.4013*x4 (28)
else
 if x2 <= 154.35
  if x1 <= 12.366
   y = 0.59979 -0.0021783*x2 -0.078047*x4 (7)
  else
   if x4 <= 0.098333
    y = 0.31092 +0.64838*x4 (11)
   else
    y = 0.19385 (3)
 else
  if x5 <= 0.31339
   if x1 <= 9.9219
    if x2 <= 155.6
     y = 0.16353 (3)
    else
     y = 0.18237 (6)
   else
    y = 0.37906 -0.00068514*x3 (5)
  else
   y = 0.10157 (3)
```

The Models (refer Fig. 8):

```
M1 = 0.66957 -0.0031293*x2 +0.38258*x4
M2 = 0.91844
M3 = 0.89938
M4 = 0.81902
M5 = 0.70902
M6 = 0.60708 -0.0015359*x2
M7 = 0.64014
M8 = 0.47126
M9 = 0.15279
M10 = 0.92135 -0.031689*x1 -0.0016546*x2 -0.4013*x4
```

M11 = 0.59979 -0.0021783*x2 -0.078047*x4
M12 = 0.31092 +0.64838*x4
M13 = 0.19385
M14 = 0.16353
M15 = 0.18237
M16 = 0.37906 -0.00068514*x3
M17 = 0.10157

REFERENCES

Adluri S, Madugula M (1996). Flexural buckling of steel angles: experimental investigation. *Journal of Structural Engineering, ASCE*, 122(3), 309-317.

AISC (2000). Load and resistance factor design specification for single-angle members. American Institute of Steel Construction, Chicago, IL.

Ayaz Y, Kocamaz AF, Karakoc MB (2015). Modeling of compressive strength and UPV of high-volume mineral-admixtured concrete using rule-based M5 rule and tree model M5' classifiers. *Construction and Building Materials*, 94, 235–240.

Barszcz AM (2014). Experimentally Assisted Modelling of the Behaviour of Steel Angle Brace, *Archives of Civil Engineering*, LX(1), 3–39.

Bashar I, Amanat KM (2014). Numerical investigation of ultimate axial capacity of eccentrically loaded steel angles. *Journal of Civil Engineering (IEB)*, 42(2), 217-232.

Bathon L, Mueller W, Kempner L Jr. (1993). Ultimate load capacity of single steel angles. *Journal of Structural Engineering, ASCE*, 119(1), 279-300.

Behnood A, Olek J, Glinicki MA (2015). Predicting modulus elasticity of recycled aggregate concrete using M5' model tree algorithm. *Construction and Building Materials*, 94, 137–147.

Bose NK, Liang P (1993). Neural Networks Fundamentals with Graphs, Algorithms, and Applications. Tata-McGraw-Hill Publishing Company Limited, New Delhi.

Breiman L, Friedman J, Stone CJ, Olshen RA (1984). Classification and Regression Trees. Chapman & Hall/CRC, USA.

Clark LA, Pregibon D (1991). Tree-based models, Statistical Models in S, Chambers JM, Hastie TJ (Eds.), Wadsworth. Pacific Grove, CA, 377–419.

Dauji S (2016). Prediction of compressive strength of concrete with decision trees. *International Journal of Concrete Technology*, 2(1), 19–29.

Elgaaly M, Dagher H, Davids W (1991). Behaviour of single angle compression members. *Journal of Structural Engineering, ASCE*, 117(12), 3720-3741.

Fisher JM (2000). Load and resistance factor design specification for single-angle members. American Institute of Steel Construction, Chicago, IL.

Garg NK, Deo MC, Kumar VS (2008). Short term prediction of coastal currents using Model Trees. *Proceedings of the Indian National Conference on Advances in Hydraulic Engineering: Hydro 2008*, India, 250-256.

Gharaei-Manesh S, Fathzadeh A, Taghizadeh-Mehrjardi R (2016). Comparison of artificial neural network and decision tree models in estimating spatial distribution of snow depth in a semi-arid region of Iran. *Cold Regions Science and Technology*, 122, 26–35.

Ishida A (1968). Experimental study on column carrying capacity of 'SHY steel' angles. Yawata Technical Report No. 265, Yawata Iron and Steel Co. Ltd., Tokyo, Japan.

Jekabsons G (2016). M5 PrimeLab: M5' regression tree, model tree, and tree ensemble toolbox for Matlab/Octave. http://www.cs.rtu.lv/jekabsons/; Downloaded on 24 December 2015.

Kim JW, Pachepsky YA (2010). Reconstructing missing daily precipitation data using regression trees and artificial neural networks for SWAT streamflow simulation. *Journal of Hydrology*, 394, 305–314.

Liu Y, Chantel S (2011). Experimental study of steel single unequal-leg angles under eccentric compression. *Journal of Constructional Steel Research*, 67(6), 919-928.

Liu Y, Hui L (2008). Experimental study of beam-column behaviour of steel single angles. Journal of Constructional Steel Research, 64, 505-514.

Liu Y, Hui L (2010). Behaviour of steel single angles subjected to eccentric axial loads. *Canadian Journal of Civil Engineering*, 37(6), 887-896.

Mueller WH, Erzurumlu H (1983). Behaviour and strength of angles in compression: an experimental investigation. Research report of Civil-Structural Engineering, Division of Engineering and Applied Science, Portland State University, Oregon.

Page CR (2005). Specification for structural steel buildings. American Institute of Steel Construction, Chicago, IL.

Quinlan JR (1993). C4.5 Programs for Machine Learning. Morgan Kaufmann Publishers Inc., San Francisco, CA, USA.

Rao SS, Kumar SRS, Kalyanaraman V (2003). Numerical study on eccentrically loaded hot rolled steel single angle struts. *Proc. Ninth International Conference on Civil and Structural Engineering Computing*, Topping, B. H. V. (Ed.) Civil-Comp Press, Stirlingshire, UK, Paper 44.

Rodriguez-Galiano V, Sanchez-Castillo M, Chica-Olmo M, Chica-Rivas M (2015). Machine learning predictive models for mineral prospectivity: An evaluation of neural networks, random forest, regression trees and support vector machines. *Ore Geology Reviews*, 71, 804–818.

Rokach L, Maimon O (2015). Data Mining with Decision trees: Theory and Applications. World Scientific, Singapore.

Sakala SSS (2004). Neural network modelling of the load-carrying capacity of eccentrically-loaded single-angle struts. *Journal of Constructional Steel Research*, 60, 965-987.

Tiryaki B (2008). Predicting intact rock strength for mechanical excavation using multivariate statistics, artificial neural networks, and regression trees. *Engineering Geology*, 99, 51–60.

Wakabayashi M, Nonaka T (1965). On the buckling strength of angles in transmission towers. *Bulletin of the Disaster Prevention Research Institute*, 15(2), No. 91, 1–18.

Wasserman PD (1993). Advanced Methods in Neural Computing. Van Nostrand Reinhold Company, New York.

Witten IH, Frank E (2000). Data Mining: Practical Machine Learning Tools and Techniques. Morgan Kaufmann, San Francisco.

Woolcock S, Kitipornchai S (1986). Design of single angle web struts in trusses. *Journal of Structural Engineering, ASCE*, 112(6), 1327-1345.

Challenge Journal of Structural Mechanics

Research Article

Dynamic instability of castellated beams subjected to transverse periodic loading

Sahar Sahib Elaiwi *, Boksun Kim, Long-yuan Li

School of Engineering, Faculty of Science and Engineering, University of Plymouth, Drake Circus, Plymouth PL4 8AA, UK

ABSTRACT

In this study, an analytical solution is developed for the investigation of free vibration, static buckling and dynamic instability of castellated beams subjected to transverse periodic loading. Bolotin's method is used to perform the dynamic instability analysis. By assuming the instability modes, the mass, stiffness, and geometric stiffness matrices are derived using the kinetic energy, strain energy and potential of applied loads. Analytical equations for determining the free vibration frequency, critical buckling moment, and excitation frequency of castellated beams are derived. In addition, the influences of the flange width of the castellated beam and the static part of the applied load on the variation of dynamic instability zones are discussed.

ARTICLE INFO

Article history:
Received 21 November 2018
Revised 24 January 2019
Accepted 11 February 2019

Keywords:
Castellated beam
Buckling
Dynamic instability
Vibration frequency

1. Introduction

Technological developments in all areas of construction are encouraging researchers and engineers as well as designers in the field to improve the performance of structural members of construction. The castellated beam is one of the steel members, which uses less material but has equal performance as the I-beam of the same size. The fabrication process of castellated beams leads to an increase of beam's depth and thus the bending strength and stiffness about the major axis without adding additional materials. This leads to use castellated beams in the long span applications subject to light or moderate loading conditions for supporting floors and roofs. However, the castellated beams have web openings, which may reduce the shear resistance of the beam. Additionally, the presence of web openings also causes a decrease of the overall sectional torsional stiffness, which may decrease the resistance of the beam to lateral-torsional buckling. Kerdal (1982) and Demirdjian (1999) reported that the torsional stiffness of the web is affected by the depth and slenderness of the beam. A number of experimental, theoretical and numerical investigations have showed the factors having an impact on castellated beam's vulnerability to lateral torsion buckling, which include the distance between the lateral restrictions to the compression stresses of the flanges; properties of the material; boundary conditions; type of cross section; type and position of the loading; quantity and distribution of the residual stresses and geometric imperfections. Previous studies investigated the lateral-torsional buckling (Kerdal and Nethercot, 1982; Mohebkhah, 2004; Korrani et al., 2010; Sonck et al., 2014; Kim et al., 2016; Kwani and Wijaya, 2017) and lateral buckling (Müller et al., 2006; Showkati et al., 2012) of castellated beams under transverse loads.

Literature survey on structural members shows that little research has been carried out on the dynamic instability of castellated beams when the applying load varies with time. In many countries, the static load still dominates the current designing of structures for castellated beams, in spite of the significance of the dynamic response to machinery loading and to extreme environmental loads; for example, wind and earthquakes, that have been considered for some time. It is acknowledged that applying dynamic load can lead to the vibration of structural members, which causes a decrease in the critical load of buckling of the members. For this reason, we should understand the effect of applying the dynamic load on the structural behaviour to avoid resonance disasters due to the dynamic instability.

* *Corresponding author*. Tel.: +44-77-21448112 ; E-mail address: sahar.elaiwi@plymouth.ac.uk (S. S. Elaiwi)
ISSN: 2149-8024 / DOI: https://doi.org/10.20528/cjsmec.2019.01.002

Limited research and studies exist on the dynamics, especially the dynamic instability of castellated beams subjected to transverse loading. Since 1960 research has been carried out on the vibration-induced buckling of beams. For instance, Morris (1965) investigated the nonlinear vibration problem of a two hinged beam-column subjected to a harmonic load of any space distribution. Hsu (1966) carried out the investigation of the dynamic stability of the elastic body with given initial conditions and reported the necessary and sufficient stability criteria in terms of trajectories in the phase space of finite dimension. Huang (1980) and Chen et al. (1991) used the Bolotin's method to examine the dynamic instability of generally orthotropic beams and thick bi-modulus beams subjected to periodic axial loads, respectively. The Routh-Hurwitz stability and the averaging method have been used by Huang and Hung (1984) to study the dynamic instability of a simply supported beam subjected to periodic axial excitation. The coupling of the first two modes was considered to investigate the instability regions and vibration amplitudes. Many researchers discussed the influences of both the natural frequencies and static buckling loads on the dynamic instability behaviour. Gürgöze (1985) conducted an investigation into the instability behaviour of a pre-twisted beam subjected to a pulsating axial load. He used the Mettler method and derived the equations describing the instability regions that could be applied with different boundary conditions. A finite element dynamic instability model of Timoshenko beams was introduced by Park (1987), which adopted the extended Hamilton's principle to build the equation of the beam transverse motion in the plane. Another study was carried out by Kar and Sujata (1991), who examined the dynamic instability of rotating beams with various different boundary conditions subjected to a pulsating axial excitation. They also discussed the influences of the boundary conditions and rotational speed on the static buckling loads and the zones of parametric instability. Yeh et al. (2004) used the harmonic balance method and the finite element method to investigate the dynamic instability problem of a sandwich beam with a constrained layer and an electro rheological fluid core subjected to an axial dynamic force. Zhu et al. (2017) presented an analytical solution to examine the free vibration, static buckling and dynamic instability of laterally-restrained zed-section purlin beams under uplift wind loading. They used the classical principle of minimum potential energy, in which the kinetic energy and strain energy of the beam and the loss of the potential energy of the applied load are evaluated by assuming instability modes. The influence of different supporting boundary conditions on the dynamic instability behaviour of beams has been also studied by Uang and Fan (2001); Yoon and Kim (2002). More recently, Zhu et al. (2018) presented a study on the dynamic buckling of cold-formed steel channel section beams under the action of uniformly distributed loading. Gao et al. (2019) provided a nondeterministic dynamic stability assessment of Euler–Bernoulli beams using Chebyshev surrogate model.

In this study, an analytical solution is developed to investigate the free vibration, static buckling and dynamic instability of castellated beams subjected to transverse periodic loading. Bolotin's method is used to perform the dynamic instability analysis. By assuming the instability modes, the mass, stiffness, and geometric stiffness matrices are derived using the kinetic energy, strain energy and potential of applied loads. Analytical equations for determining the free vibration frequency, critical buckling moment, and excitation frequency of castellated beams are derived. In addition, the influences of the flange width of the castellated beam and the static part of the applied load on the variation of dynamic instability zones are discussed.

2. Governing Equations for Dynamic Instability Analysis of Castellated Beams

The analysis model used for this study is illustrated in Fig. 1(a). The cross-section of the castellated beam is assumed to be doubly symmetric, with the flange width and thickness as b_f and t_f, the web depth and thickness as h_w and t_w, and the half depth of hexagons as a. The half of the distance between the centroids of the two T-sections is e. The side length of the hexagonal opening is $\left(2a/\sqrt{3}\right)$, and the hexagonal opening height is $2a$, respectively.

According to Fig. 1(b), the lateral and transverse displacements of the beam are assumed to be v(x) and w(x), respectively, and the angle of twist of the cross-section is $\phi(x)$. The strain energy of the beam involves two parts; the strain energy generated by the bending and the strain energy generated by the twist.

In order to consider the warping influence, the cross-section of the castellated beam is decomposed into three parts, two of which represent the top and bottom T-sections, one of which represents the middle-part of the web. It is assumed that the displacements at the shear canters of the top and bottom tee-sections are small and can be expressed as follows (see Fig. 1) (Kim et al., 2016):

$$v_1(x) = v(x) + \frac{h}{2}\phi(x) \tag{1}$$

$$v_2(x) = v(x) - \frac{h}{2}\phi(x) \tag{2}$$

$$w_1(x) = w + \frac{h}{2}(1 - cos\phi) \approx w \tag{3}$$

$$w_2(x) = w + \frac{h}{2}(1 - cos\phi) \approx w \tag{4}$$

where v_1 and v_2 are the lateral displacements of the shear centers of the top and bottom T-sections, w_1 and w_2 are the transverse displacements of the shear centers of the top and bottom T-sections, h is the distance between the shear centers of top and bottom T-sections. The kinetic energy, T, of the castellated beam due to the lateral and transverse displacements, and the rotation of the section thus can be expressed as:

The kinetic energy for the top T- section:

$$T_{top} = \frac{\rho A_{tee}}{2}\int_0^l (\dot{v_1}^2 + \dot{w_1}^2)dx + \frac{\rho I_{ptop}}{2}\int_0^l \dot{\phi}^2\, dx \tag{5}$$

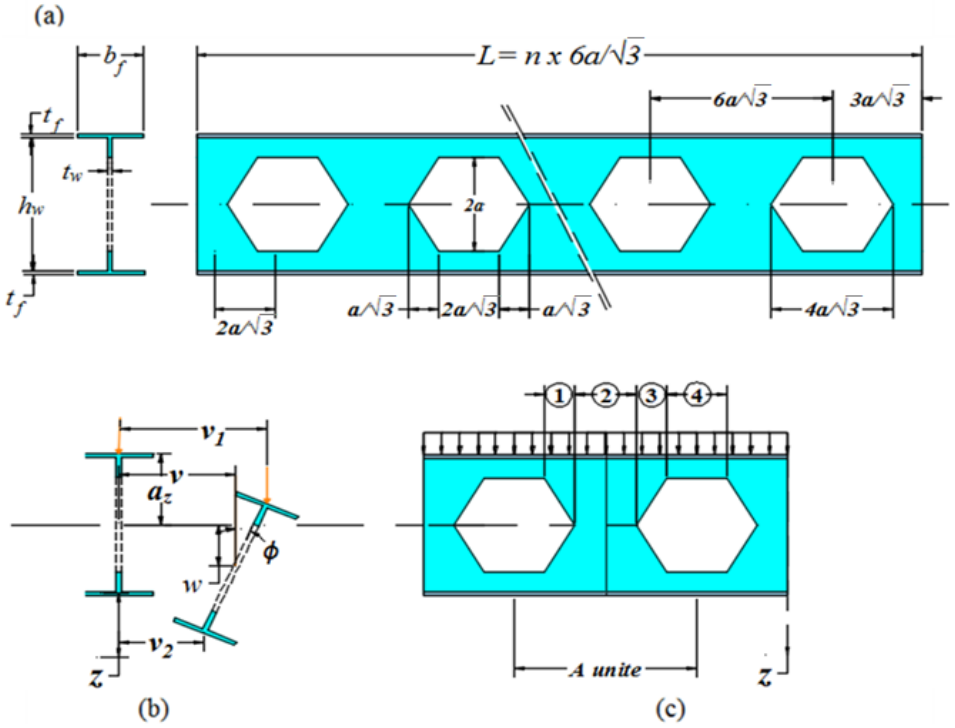

Fig. 1. (a) Notations used in castellated beams; (b) Loading and displacements of web and displacement of flanges when lateral–torsional buckling occurred; (c) Section properties of middle-part of web in four different regions. ($I_{y3} = I_{y3}^*$, $I_{z3} = I_{z3}^*$, $J_3 = J_3^*$ in region 2, in region 4, $I_{y3} = I_{z3} = J_3 = 0$, section properties vary with x in regions 1 and 3.)

The kinetic energy for the bottom T- section:

$$T_{bot} = \frac{\rho A_{tee}}{2}\int_0^l (\dot{v_2}^2 + \dot{w_2}^2)dx + \frac{\rho I_{pbot}}{2}\int_0^l \dot{\phi}^2\, dx \qquad (6)$$

The kinetic energy for the middle part between the two T- sections:

$$T_{web} = \frac{\rho 2at_w}{2}\int_0^l (\dot{v}^2 + \dot{w}^2)dx + \frac{\rho I_{pweb}}{2}\int_0^l \dot{\phi}^2\, dx \qquad (7)$$

Hence, the total kinetic energy of the beam is:

$$T = \frac{\rho}{2}\left[A_{tee}\left[\int_0^l (\dot{v_1}^2 + \dot{w_1}^2)dx + \int_0^l (\dot{v_2}^2 + \dot{w_2}^2)dx\right] + at_w\int_0^l (\dot{v}^2 + \dot{w}^2)dx + I_p\int_0^l \dot{\phi}^2\, dx\right] \qquad (8)$$

where ρ is the density, l is the beam length, $A_{tee} = b_f t_f + t_w(h_w/2 - a)$ is the cross-section area of the T-section, $I_p = I_{pbot} + I_{pweb} + I_{ptop}$ is the polar moment of inertia. Note that the dot above a symbol in above equations represents the derivative of the symbol with respect to time.

The strain energy of the castellated beam is also determined based on the three parts due to the transverse displacement, lateral displacement and rotation. It thus can be written as follows:

$$U_s = \frac{1}{2}\int_0^l \left[EI_{y1}\left(\frac{d^2w_1}{dx^2}\right)^2 + EI_{z1}\left(\frac{d^2v_1}{dx^2}\right)^2 + GJ_1\left(\frac{d\phi}{dx^2}\right)^2\right]dx + \frac{1}{2}\int_0^l \left[EI_{y2}\left(\frac{d^2w_2}{dx^2}\right)^2 + EI_{z2}\left(\frac{d^2v_2}{dx^2}\right)^2 + GJ_2\left(\frac{d\phi}{dx^2}\right)^2\right]dx + \frac{1}{2}\int_0^l \left[EI_{y3}\left(\frac{d^2w_3}{dx^2}\right)^2 + EI_{z3}\left(\frac{d^2v_3}{dx^2}\right)^2 + GJ_3\left(\frac{d\phi}{dx^2}\right)^2\right]dx \qquad (9)$$

where U_s is the strain energy, E is the Young's modulus, G is the shear modulus. $I_{y1} = I_{y2}$ and $I_{z1} = I_{z2}$ are the second moments of the T- sectional area about the y and z axes. $J_1 = J_2$ is the torsional constant of the T-section, I_{y3} and I_{z3} are the second moments of the cross-sectional area of the mid-part of the web about the y and z axes, respectively, and J_3 is the torsional constant of the mid-part of the web.

Hence, the formula of the strain energy of castellated beam (top T- sections, bottom T- sections and mid-part of the web) can be written as follows:

$$U = \frac{1}{2}\int_0^l \left[2EI_{y1}\left(\frac{d^2w_1}{dx^2}\right)^2 + 2EI_{z1}\left(\frac{d^2v_1}{dx^2}\right)^2 + \frac{h^2}{2}EI_{z1}\left(\frac{d^2\phi}{dx^2}\right)^2 + 2GJ_1\left(\frac{d\phi}{dx^2}\right)^2\right]dx + \frac{1}{2}\int_0^l \left[EI_{y3}\left(\frac{d^2w_2}{dx^2}\right)^2 + EI_{z3}\left(\frac{d^2v_2}{dx^2}\right)^2 + GJ_3\left(\frac{d\phi}{dx^2}\right)^2\right]dx \qquad (10)$$

According to Fig. 1, I_{y1}, I_{z1} and J_1 are constants, whereas I_{y3}, I_{z3} and J_3 are the function of x and dependent upon the location of the web openings. Note, from the comparison between equation of the strain energy of an I-beam without web openings and Eq. (10), the following relations can be obtained:

$$I_y = 2I_{y1} + I_{y3} \qquad (11)$$

$$I_z = 2I_{z1} + I_{z3} \qquad (12)$$

$$I_w = \left(\frac{h}{2}\right)^2 I_z \approx \frac{h^2}{2}I_{z1} \qquad (13)$$

$$J = 2J_1 + J_3 \tag{14}$$

$$I_p = I_y + I_z = 2I_{y1} + 2I_{z1} + kI_{y3} + kI_{z3} \tag{15}$$

According to the work (Kim et al., 2016), k refers to the fraction of the volume of the solid and holes in the mid-part of the web. In castellated beams, because of matching of the solid areas and holes in the mid-part of the web, the value of k=0.5 is taken.

Assume that the transverse load is the periodic load applying on the top flange of castellated beam when the sheeting is fixed with the top flange (e.g. for wind-induced vibration). In this case, the loss of potential energy V of the transverse load q_z can be expressed as follows:

$$V = \int_0^l \left[M_y \phi \left(\frac{d^2 v}{dx^2} \right) + \frac{a_z q_z}{2} \phi^2 \right] dx \tag{16}$$

where q_z is the distribution load, M_y is the pre-buckling internal bending moment, and a_z refers to the z-coordinate of the loading point, which is equal to the distance between the loading point and the shear centre of the beam. In the present case, $a_z = h_w/2 + t_f$ because the uniformly distributed load is applied on the top flange of the beam. The second term in Eq. (16) is attributed to the effect of loading position, which, in the present case, has a positive effect on the stability of the beam and thus will increase the critical buckling load.

According to the Lagrange method, the equations of motion describing the lateral-torsional buckling of the beam can be expressed as follows:

$$\frac{d}{dt}\left(\frac{\partial L}{\partial \dot{q}}\right) - \frac{\partial L}{\partial q} = 0 \tag{17}$$

where $L = T - (U - V)$ is the Lagrangian function, and q is the general displacement vector. Substituting Eqs. (1-4), (8), (10), (16) into (17), the governing equation for the dynamic instability analysis of a castellated beam is obtained as follows (Kratzig and Nawrotzki, 1991; Li, 1991; Patel et al., 2006).

$$[\boldsymbol{M}]\{\ddot{\boldsymbol{q}}\} + [\boldsymbol{K}]\{\boldsymbol{q}\} - \lambda\left[\boldsymbol{K_g}\right]\{\boldsymbol{q}\} = \{0\} \tag{18}$$

where **[M]** is the mass matrix, **[K]** is the elastic stiffness matrix, $\mathbf{[K_g]}$ is the geometric stiffness matrix, $\{\ddot{\mathbf{q}}\}$ is the generalized acceleration vector, $\{\mathbf{q}\}$ is the general displacement vector, and λ is the loading factor. The mass, stiffness, and geometric stiffness matrices are expressed as follows:

$$[\boldsymbol{M}] = \begin{bmatrix} \frac{\partial^2 T}{\partial \dot{q}_1^2} & \frac{\partial^2 T}{\partial \dot{q}_1 \partial \dot{q}_2} & \frac{\partial^2 T}{\partial \dot{q}_1 \partial \dot{q}_3} \\ \frac{\partial^2 T}{\partial \dot{q}_2 \partial \dot{q}_1} & \frac{\partial^2 T}{\partial \dot{q}_2^2} & \frac{\partial^2 T}{\partial \dot{q}_2 \partial \dot{q}_3} \\ \frac{\partial^2 T}{\partial \dot{q}_3 \partial \dot{q}_1} & \frac{\partial^2 T}{\partial \dot{q}_3 \partial \dot{q}_2} & \frac{\partial^2 T}{\partial \dot{q}_3^2} \end{bmatrix} \tag{19}$$

$$[\boldsymbol{K}] = \begin{bmatrix} \frac{\partial^2 U}{\partial q_1^2} & \frac{\partial^2 U}{\partial q_1 \partial q_2} & \frac{\partial^2 U}{\partial q_1 \partial q_3} \\ \frac{\partial^2 U}{\partial q_2 \partial q_1} & \frac{\partial^2 U}{\partial q_2^2} & \frac{\partial^2 U}{\partial q_2 \partial q_3} \\ \frac{\partial^2 U}{\partial q_3 \partial q_1} & \frac{\partial^2 U}{\partial q_3 \partial q_2} & \frac{\partial^2 U}{\partial q_3^2} \end{bmatrix} \tag{20}$$

$$\left[\boldsymbol{K_g}\right] = \begin{bmatrix} \frac{\partial^2 V}{\partial q_1^2} & \frac{\partial^2 V}{\partial q_1 \partial q_2} & \frac{\partial^2 V}{\partial q_1 \partial q_3} \\ \frac{\partial^2 V}{\partial q_2 \partial q_1} & \frac{\partial^2 V}{\partial q_2^2} & \frac{\partial^2 V}{\partial q_2 \partial q_3} \\ \frac{\partial^2 V}{\partial q_3 \partial q_1} & \frac{\partial^2 V}{\partial q_3 \partial q_2} & \frac{\partial^2 V}{\partial q_3^2} \end{bmatrix} \tag{21}$$

Assume that the externally applied load q_z is periodic loading, in which case the loading factor can be divided into two parts as expressed as follows:

$$\lambda = \lambda_s + \lambda_t \cos\Omega t \tag{22}$$

where λ_s and λ_t are the amplitudes of the static and dynamic parts, respectively, Ω is the excitation frequency of the dynamic part of the load, and t is the time.

The dynamic instability regions of the beam described by Eq. (18) can be calculated by investigating periodic solutions with the periods of $T=2\pi/\Omega$ and $2T=4\pi/\Omega$. The solution with the period of 2T is of particular importance, representing the primary instability region of the structure, which can be expressed using the form of trigonometric series given by:

$$\{\boldsymbol{q}\} = \sum_{k=1,3,\ldots} \left[\{\boldsymbol{a_k}\} \sin\frac{k\Omega t}{2} + \{\boldsymbol{b_k}\} \cos\frac{k\Omega t}{2} \right] \tag{23}$$

where $\{\boldsymbol{a_k}\}$ and $\{\boldsymbol{b_k}\}$ are the vectors of coefficients of the assumed solution. Substituting Eqs. (22) and (23) into (18) and letting the coefficients of the series associated with $\sin(\Omega t/2)$ and $\cos(\Omega t/2)$ be zero, it yields:

$$\left([\boldsymbol{K}] - \frac{2\lambda_s - \lambda_t}{2}\left[\boldsymbol{K_g}\right] - \frac{\Omega^2}{4}[\boldsymbol{M}] \right)\{\boldsymbol{a_1}\} = \{\boldsymbol{0}\} \tag{24}$$

$$\left([\boldsymbol{K}] - \frac{2\lambda_s + \lambda_t}{2}\left[\boldsymbol{K_g}\right] - \frac{\Omega^2}{4}[\boldsymbol{M}] \right)\{\boldsymbol{b_1}\} = \{\boldsymbol{0}\} \tag{25}$$

For given values of λ_s and λ_t one can calculate the two frequencies of Ω from Eqs. (24) and (25), which represent the boundary of dynamic instability region of the castellated beams under periodic loading.

3. Simply Supported, Doubly Symmetric Castellated Beam subjected to Periodic Loads on Top Flange

For the calculation due to the dynamic lateral-torsional buckling, the displacement functions *w(x)*, *v(x)*, $\phi(x)$ and pre-buckling internal bending moment $M_y(x)$ that satisfy the boundary conditions of a simply supported beam can be assumed as follows:

$$v(x) = q_1(t)sin\frac{\pi x}{l} \quad (26)$$

$$w(x) = q_2(t)sin\frac{\pi x}{l} \quad (27)$$

$$\phi(x) = q_3(t)sin\frac{\pi x}{l} \quad (28)$$

$$M_y(x) = \frac{q_z x(l-x)}{2} \quad (29)$$

where $q_i(t)$ $(i = 1,2,3)$ are the functions of time *t*.

Therefore, the mass, stiffness, and geometric stiffness matrices for simply supported beam are obtained from Eqs. (19-21) and are expressed as follows:

$$[\boldsymbol{M}] = \begin{bmatrix} m_{11} & 0 & 0 \\ 0 & m_{22} & 0 \\ 0 & 0 & m_{33} \end{bmatrix} \quad (30)$$

where:

$$m_{11} = m_{22} = \rho l(at_w + A_{tee}) \quad (31)$$

$$m_{33} = \rho l\left(\frac{A_{tee}h^2}{4} + \frac{I_p}{2}\right) \quad (32)$$

$$[\boldsymbol{K}] = \begin{bmatrix} \kappa_{11} & 0 & 0 \\ 0 & \kappa_{22} & 0 \\ 0 & 0 & \kappa_{33} \end{bmatrix} \quad (33)$$

where:

$$\kappa_{11} = \frac{El(2I_{z1}+kI_{z3})}{2}\left(\frac{\pi}{l}\right)^4 \quad (34)$$

$$\kappa_{22} = \frac{El(2I_{y1}+kI_{y3})}{2}\left(\frac{\pi}{l}\right)^4 \quad (35)$$

$$\kappa_{33} = \frac{EI_w l}{2}\left(\frac{\pi}{l}\right)^4 + \frac{Gl(2J_1+kJ_3)}{2}\left(\frac{\pi}{l}\right)^2 \quad (36)$$

$$\left[\boldsymbol{K_g}\right] = \begin{bmatrix} 0 & 0 & \kappa_{g13} \\ 0 & 0 & 0 \\ \kappa_{g31} & 0 & \kappa_{g33} \end{bmatrix} \quad (37)$$

where:

$$\kappa_{g13} = \kappa_{g31} = -\frac{q_z l}{8}\left(\frac{\boldsymbol{\pi^2}}{\boldsymbol{3}} + 1\right), \kappa_{g33} = -\frac{a_z q_z l}{2} \quad (38)$$

3.1. Free vibration analysis

The free vibration frequency of the lateral-torsional vibration of the castellated beam can be determined using Eq. (39):

$$\|[\boldsymbol{K}] - \omega^2[\boldsymbol{M}]\| = 0 \quad (39)$$

where ω is the free vibration frequency. Substituting Eqs. (30-33) into (39), the following frequency can be obtained:

$$\omega_1 = \left(\frac{\pi}{l}\right)^2\sqrt{\frac{E(2I_{z1}+kI_{z3})}{2\rho(at_w+A_{tee})}} \quad (40)$$

$$\omega_2 = \left(\frac{\pi}{l}\right)^2\sqrt{\frac{E(2I_{y1}+kI_{y3})}{2\rho(at_w+A_{tee})}} \quad (41)$$

$$\omega_3 = \left(\frac{\pi}{l}\right)^2\sqrt{\frac{2\left(EI_w+\frac{Gl^2}{\pi^2}(2J_1+kJ_3)\right)}{\rho(A_{tee}h^2+2I_p)}} \quad (42)$$

I^*_{z3} can be negligible because in most of castellated beams $I^*_{z3} << 2I_{z1}$, then Eqs. (40-42) can be simplified as follows:

$$\omega_1 = \left(\frac{\pi}{l}\right)^2\sqrt{\frac{E(2I_{z1})}{2\rho(at_w+A_{tee})}} \quad (43)$$

$$\omega_2 = \left(\frac{\pi}{l}\right)^2\sqrt{\frac{E(2I_{y1})}{2\rho(at_w+A_{tee})}} \quad (44)$$

$$\omega_3 = \left(\frac{\pi}{l}\right)^2\sqrt{\frac{2\left(EI_w+\frac{Gl^2}{\pi^2}(2J_1+kJ_3)\right)}{\rho(A_{tee}h^2+2(I_{z1}+I_{y1}))}} \quad (45)$$

The above formulations (43), (44) and (45) give the natural frequencies, which are well known and can be found from many vibration textbooks. These equations represent the translational and rotational vibrations of castellated beams. Moreover, it indicates that the lateral vibration and torsional vibration modes are influenced by the web openings.

3.2. Buckling analysis

The critical load of the lateral-torsional buckling of the castellated beam subjected to a static load can be calculated using Eq. (46):

$$\|[\boldsymbol{K}] - \lambda_{cr}[\boldsymbol{K_g}]\| = 0 \quad (46)$$

where λ_{cr} is the loading factor and $q_{cr} = \lambda_{cr}q_z$ is the critical load for static buckling.

Substituting Eqs. (33) and (37) into (46), the following critical load is obtained:

$$\lambda_{cr} = -\frac{K_{11}K_{g33} \pm \sqrt{{K_{11}}^2{K_{g33}}^2 + 4{K_{g13}}^2K_{11}K_{33}}}{2{K_{g13}}^2} \quad (47)$$

$$\left(\frac{q_z l^2}{8}\right)_{cr} = \frac{\left(\left(\frac{h_w}{2}+t_f\right) + \sqrt{\left(\frac{h_w}{2}+t_f\right)^2 + \frac{1}{4}\left(l_w + \frac{G(2J_1+kJ_3)}{E}\left(\frac{l}{\pi}\right)^2\right)\left(\frac{\pi^2}{3}+1\right)^2 \times \frac{1}{(2I_{z1}+I_{z3})}}\right)}{\left(\frac{1}{3}+\frac{1}{\pi^2}\right)^2} \times \frac{2E(2I_{z1}+I_{z3})}{l^2} \quad (48)$$

$$\left(\frac{q_z l^2}{8}\right)_{cr} = \frac{\left(\left(\frac{h_w}{2}+t_f\right)+\sqrt{\left(\frac{h_w}{2}+t_f\right)^2+\frac{1}{4}\left(I_w+\frac{G(2J_1+kJ_3)}{E}\left(\frac{l}{\pi}\right)^2\right)\left(\frac{\pi^2}{3}+1\right)^2\times\frac{1}{(2I_{z1})}}\right)}{\left(\frac{1}{3}+\frac{1}{\pi^2}\right)^2} \times \frac{2E(2I_{z1})}{l^2} \quad (49)$$

It can be noticed that Eq. (49) is similar to the formulation of the critical load given in the work (Kim et al., 2016) for simply supported castellated beams when the load is applied at the top flange.

3.3. Dynamic instability

The dynamic instability region of the castellated beam can be calculated using Eq. (50):

$$\left\|[\boldsymbol{K}]-\frac{2\lambda_s\pm\lambda_t}{2}[\boldsymbol{K_g}]-\frac{\Omega^2}{4}[\boldsymbol{M}]\right\|=0 \quad (50)$$

Substituting Eqs. (30-37) into (50), it yields:

$$\frac{\Omega^2}{4} = \frac{(K_{33}^* m_{11}+K_{11}m_{33})\pm\sqrt{\left(K_{11}m_{33}-K_{33}^* m_{11}\right)^2+4\left(\frac{2\lambda_s\pm\lambda_t}{2}\right)^2 {K_{g13}}^2 m_{33}m_{11}}}{2m_{33}m_{11}} \quad (51)$$

where

$$K_{33}^* = K_{33}-\frac{2\lambda_s\pm\lambda_t}{2}K_{g33} \quad (52)$$

It can be seen that, there are four different equations given by Eq. (51), which represent four different Ω values, where the value of Ω^2 is associated with vibration modes, which were illustrated in the free vibration analysis shown in Section 3.1.

4. Comparison of the Dynamic Instability of Simply Supported Beams due to Transverse Periodic Loading

Table 1 gives the dimensions and material properties of four castellated beams of different flange widths (b_f=100 mm, b_f =150 mm, b_f =200 mm, and b_f =250 mm). The analytical solutions used to determine the natural frequencies are obtained directly from Eqs. (43-45); while the critical loads are obtained by Eq (49).

Figs. 2-4 present the variation of the frequencies of lateral vibration, vertical vibration and rotational vibration of the beams of different flange widths versus the beam length. The three figures correspond to the 1st, 2nd and 3rd vibration modes.

From these figures it can be observed that, for each vibration mode, the frequency curves have a similar variation pattern. In addition, the beam length and the flange width influence the frequencies. Increasing the beam length causes a reduction in the frequencies. In contrast, the larger flange width gives the greater frequencies. Furthermore, it can be seen from the figures that the frequency of the lateral vibration is slightly higher than the frequency of the rotational vibration of the beam but a little higher than the frequency of the vertical vibration of the castellated beam.

Table 1. Table.

b_f mm	t_f mm	h_w mm	t_w mm	a mm	E GPa	ρ kg/m³	σ_y MPa	G GPa	v
100	10	300	8	100	210	7800	275	78	0.3
150	10	300	8	100	210	7800	275	78	0.3
200	10	300	8	100	210	7800	275	78	0.3
250	10	300	8	100	210	7800	275	78	0.3

Note*: Dynamic instability analysis uses four different beam lengths. They are 4.156 m; 6.235 m; 9.006 m and 14.549 m

Fig. 5 plots the critical load curves of the beams of different flange widths subjected to the transverse static load applying on the top flange, where the critical moment has been normalized using the yield moment,

$M_y = \frac{2\sigma_y I_{reduced}}{h_w+2t_f}$,

where

$I_{reduced} = \frac{b_f(h_w+2t_f)^3}{12} - \frac{(2a)^3 t_w}{12} - \frac{(h_w)^3(b_f-t_w)}{12}$.

It can be noticed, as expected, that for each beam the increase of beam length causes the reduction of the critical moment.

Figs. 6-9 show the dynamic instability zones of the castellated beams with four different flange widths, subjected to transverse periodic load applied at the top flange of the beam, in which the geometric stiffness matrix is assessed using the static critical load, that is

$q_y = q_{cr}$,

where

$q_y = 16\frac{\sigma_y I_{reduced}}{l^2(h_w+2t_f)}$.

The four figures correspond to four different beam lengths as indicated in Table 1. It can be observed from these figures that, the dynamic instability regions of the four beams all exhibit a "v" shape despite of having different flange widths. With the increase of beam length, the dynamic instability zone not only moves towards to higher frequency side but its width is also expanded. In contrast, where the beam length is the same, the width of the dynamic instability zone decreases with the increase of the flange width.

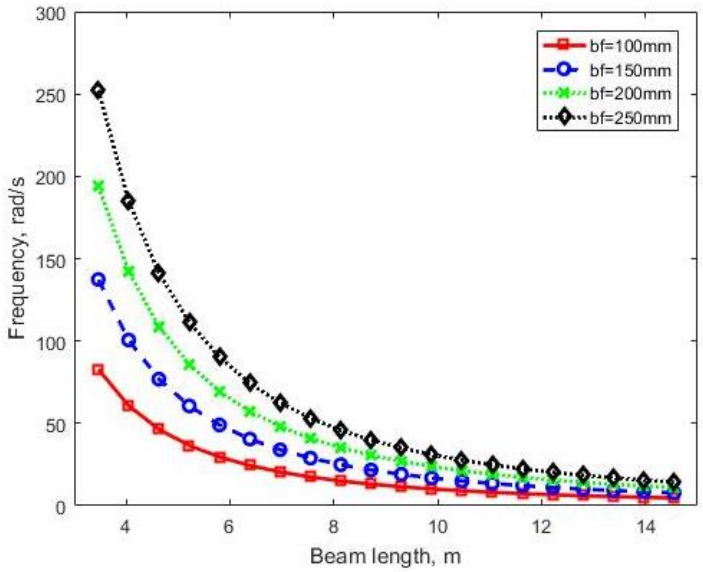

Fig. 2. Comparison of frequencies for simply supported castellated beams with different flange widths (1st mode).

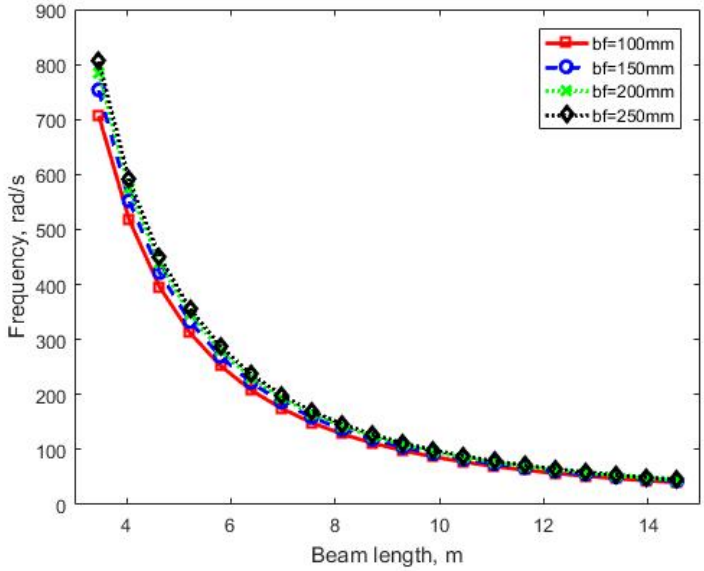

Fig. 3. Comparison of frequencies for simply supported castellated beams with different flange widths (2nd mode).

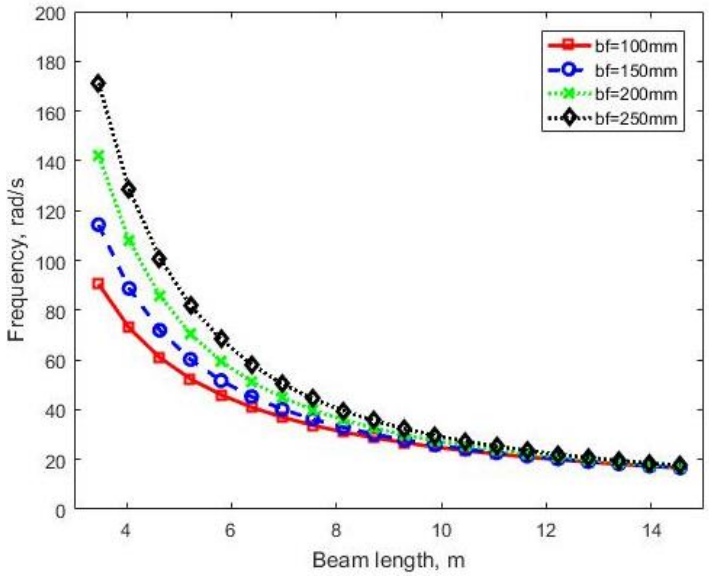

Fig. 4. Comparison of frequencies for simply supported castellated beams with different flange widths (3rd mode).

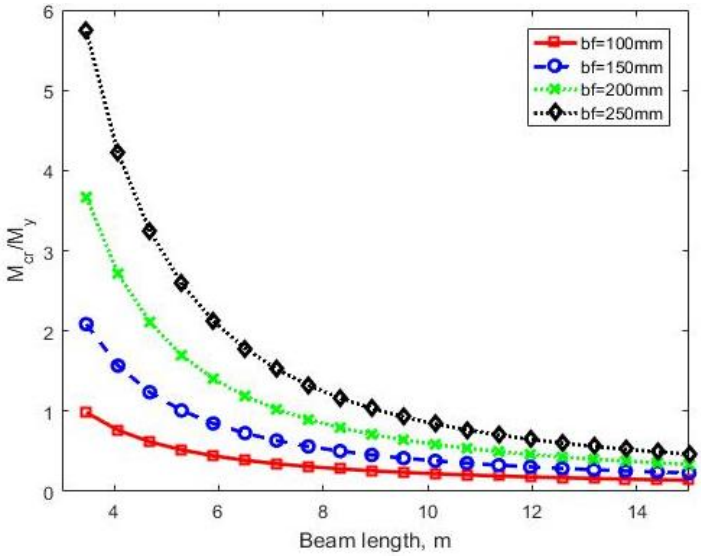

Fig. 5. Comparison of critical buckling moments of simply supported castellated beams with different flange widths.

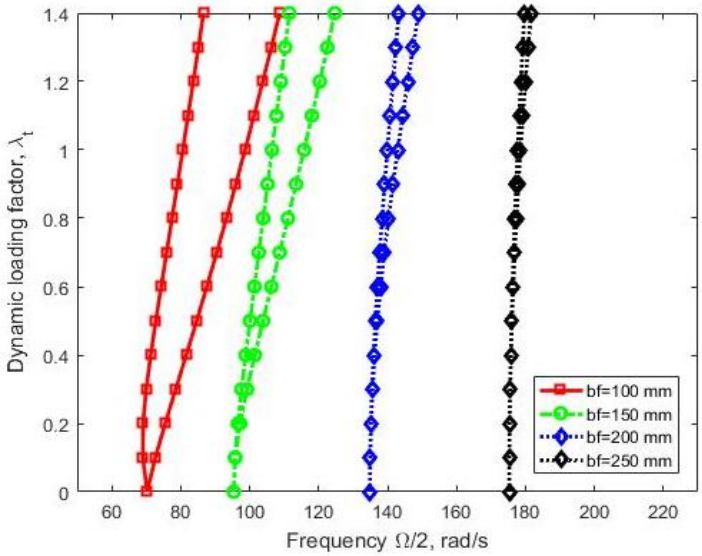

Fig. 6. Comparison of dynamic instability regions of simply supported castellated beams (beam length 4.156 meter) ($q_y = q_{cr}$ and $\lambda_s = 0$).

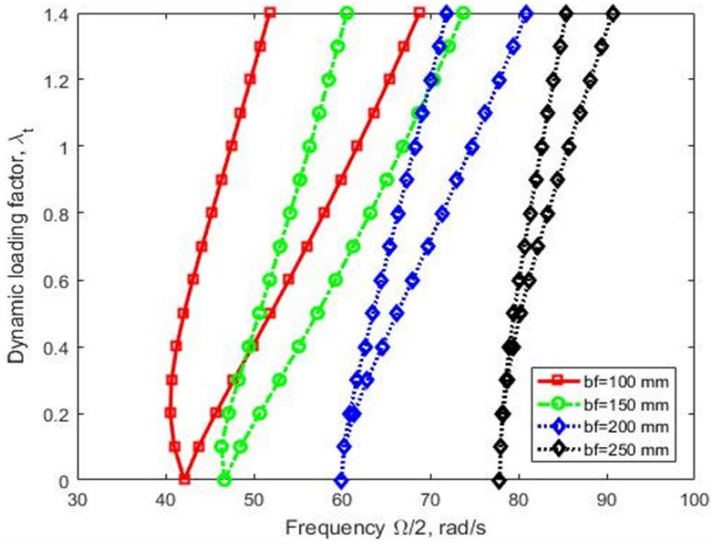

Fig. 7. Comparison of dynamic instability regions of simply supported castellated beams (beam length 6.235 meter) ($q_y = q_{cr}$ and $\lambda_s = 0$).

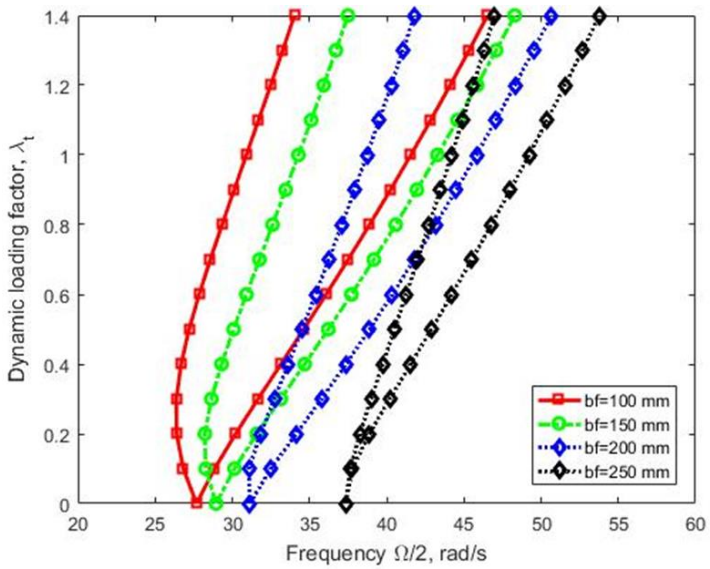

Fig. 8. Comparison of dynamic instability regions of simply supported castellated beams (beam length 9.006 meter) ($q_y = q_{cr}$ and $\lambda_s = 0$).

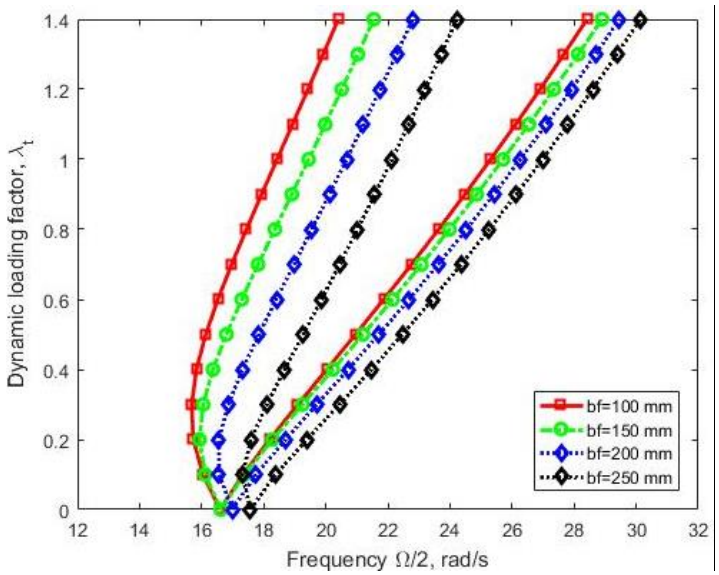

Fig. 9. Comparison of dynamic instability regions of simply supported castellated beams (beam length 14.549 meter) ($q_y = q_{cr}$ and $\lambda_s = 0$).

5. Conclusions

This study has provided an analytical study on the dynamic instability of castellated beams subjected to transverse periodic loading at top flange. The dynamic instability analysis employed in the present study uses Bolotin's method, while the mass, stiffness, and geometric stiffness matrices are derived using the kinetic energy, strain energy and the potential of applied loads. From the obtained results the following conclusions can be drawn:

- The free vibration, static buckling and dynamic instability analyses of castellated beams subjected to transverse periodic loading at the top flange are influenced by the coupling between the translational and rotational modes.
- Increasing the flange width of beam leads to the increase of both the frequency and critical buckling moment. However, increasing beam length reduces this effect.
- The dynamic instability zone of the castellated beam will move towards to high-frequency side and the corresponding width of the dynamic instability zone decreases when its flanges become wide.
- The effect of lateral torsional buckling on the dynamic instability zone becomes more significant in the short beam than in the long beam; and also in the wide flange beam than in the narrow flange beam.

Acknowledgements

The first author is grateful to the Ministry of Higher Education and Scientific Research in Iraq to the financial support of her Ph.D study at the University of Plymouth.

REFERENCES

Bolotin VV (1964). The Dynamic Stability of Elastic Systems. San Francisco, CA, Holden-day, Inc.

Yeh JY, Chen LW, Wang CC (2004). Dynamic stability of a sandwich beam with a constrained layer and electrorheological fluid core. *Composite Structures*, 64(1), 47-54.

Chen LY, Lin PD, Chen LW (1991). Dynamic stability of thick bimodulus beams. *Computers & Structures*, 41(2), 257-263.

Demirdjia S (1999). Stability of Castellated Beam Webs. *Ph.D thesis*, McGill University Montreal, Canada.

Gao K, Gao W, Wu BH, Song CM (2019). Nondeterministic dynamic stability assessment of Euler–Bernoulli beams using Chebyshev surrogate model. *Applied Mathematical Modelling*, 66, 1-25.

Gürgöze M (1985). On the dynamic stability of a pre-twisted beam subject to a pulsating axial load. *Journal of Sound and Vibration*, 102(3), 415-422.

Hsu CS (1966). On dynamic stability of elastic bodies with prescribed initial conditions. *International Journal of Engineering Science*, 4(1), 1-21.

Huang CC (1980). Dynamic stability of generally orthotropic beams. *Fibre Science and Technology*, 13(3), 187-198.

Huang JS, Hung LH (1984). Dynamic stability for a simply supported beam under periodic axial excitation. *International Journal of Nonlinear Mechanics*, 19(4), 287-301.

Kar RC, Sujata T (1991). Dynamic stability of a rotating beam with various boundary conditions. *Computers & Structures*, 40(3), 753-773.

Kazemi Nia Korrani HR, Kabir MZ, Molanaei S (2010). Lateral Torsional Buckling of Castellated Beams Under End Moments. Amirkabir University of Technology.

Kerdal D (1982). Lateral-torsional buckling strength of castellated beams. *Ph.D thesis*, Civil and Structural Engineering, Faculty of Engineering (Sheffield), University of Sheffield, Sheffield, UK.

Kim B, Li LY, Edmonds A (2016). Analytical solutions of lateral-torsional buckling of castellated beams. *International Journal of Structural Stability and Dynamics*, 16(8), 1-16 (1550044).

Kratzig WB, Li LY, Nawrotzki P (1991). Stability conditions for non-conservative dynamical systems. *Computational Mechanics*, 8(3), 145-151.

Kwani S, Wijaya PK (2017). Lateral torsional buckling of castellated beams analyzed using the collapse analysis. *Procedia Engineering*, 171, 813–820.

Lagerqvist O, Hedman-Pétursson E, Unosson E, Feldmann M (2006). Large web openings for service integration in composite floors. Design Guide (En), Technical Steel Report.

Li LY (1991). Interaction of forced and parametric loading vibrations. *Computers & Structures*, 40(3), 615-618.

Mohebkhah A (2004). The moment-gradient factor in lateral–torsional buckling on inelastic castellated beams. *Journal of Constructional Steel Research*, 60(10), 1481-1494.

Morris NF (1965). The dynamic stability of beam-columns with a fixed distance between supports. *Journal of the Franklin Institute*, 280(2), 163-173.

Müller C, Hechler O, Bureau A, Bitar D, Joyeux D, Cajot LG, Demarco T, Lawson RM, Hicks S, Devine P, Showkati H, Ghazijahani TG, Noori A, Zirakian T (2012). Experiments on elastically braced castellated beams. *Journal of Constructional Steel Research*, 77, 163-172.

Nethercot D, Kerdal D (1982). Lateral-torsional buckling of castellated beams. *The Structural Engineer*, 60B(3), 53-61.

Park YP (1987). Dynamic stability of a free Timoshenko beam under a controlled follower force. *Journal of Sound and Vibration*, 113(3), 407-415

Patel SN, Datta PK, Sheikh AH (2006). Buckling and dynamic instability analysis of stiffened shell panels. *Thin-Walled Structures*, 44(3), 321-333.

Showkati H, Ghazijahani TG, Noori A, Zirakian T (2012). Experiments on elastically braced castellated beams. *Journal of Constructional Steel Research*, 77, 163-172.

Sonck D, Van Impe R, Belis J (2014). Experimental investigation of residual stresses in steel cellular and castellated members. *Construction and Building Materials*, 54, 512-519.

Uang CM, Fan CC (2001). Cyclic stability criteria for steel moment connections with reduced beam section. *Journal of Structural Engineering*, 127(9), 1021-1027.

Yoon SJ, Kim JH (2002). A concentrated mass on the spring unconstrained beam subjected to a thrust. *Journal of Sound and Vibration*, 254(4), 621-634.

Zhu J, Qian S, Li LY (2017). Dynamic instability of laterally-restrained zed-purlin beams under uplift loading. *International Journal of Mechanical Sciences*, 131–132, 408–413.

Zhu J, Qian S, Li LY (2018). Dynamic instability of channel-section beams under periodic loading. *Mechanics of Advanced Materials and Structures*, (in press).

Challenge Journal of Structural Mechanics

Research Article

Improving the impact resistance of recycled aggregate concretes with different types of fibers

Muhammet Gökhan Altun, Meral Oltulu *

Department of Civil Engineering, Atatürk University, 25240 Erzurum, Turkey

ABSTRACT

In this study, the aim was to use different types of fibers to improve the impact resistance of recycled aggregate concrete (RAC) that normally shows poor performance against mechanical impacts compared to normal concrete (NC). For this purpose, 18 groups of concrete were cast using different parameters. The study examined different types of concrete mixtures where the proportion of RCA (recycled coarse aggregate) used was 30% and 50% respectively, and where steel fiber-reinforcement was used in proportions of 1% and 2%, and polypropylene fiber-reinforcement was used in proportions of 0.1%. While the material performance of RAC compared to NC is analyzed in existing published literature, there is no evidence on whether the use of RCA and hybrid fibers affect the impact properties of concrete. Drop weight impact testing was conducted on test specimens and the impact resistance of these specimens was studied at 28 days. It was observed that the increasing use of RCA reduced the impact resistance. The use of 30% RCA does not significantly influence the strength of concrete. According to the results, the performance of both the NC and RAC was increased with an increase in the volume fractions of steel fiber used. In addition, hybrid fiber-reinforced concretes showed the best results of all the concrete groups.

ARTICLE INFO

Article history:
Received 17 January 2019
Revised 5 March 2019
Accepted 10 March 2019

Keywords:
Recycled aggregate
Impact resistance
Polypropylene fiber
Steel fiber
Hybrid fiber

1. Introduction

Recycled aggregates (RAs) obtained from demolished concrete structures are generally used as filler material in roads and in groundwork, and it can also be used in lean concrete and NC instead of, or with, natural aggregates. In the past, the reason why RAs were not widely used in concrete production was because they exhibited weaker mechanical properties than natural aggregates. But recently, diminishing natural resources and the importance of sustainability has meant that studies about the use of RAs in concrete have become popular (Khalaf and Devenny, 2004; Oikonomou, 2005; Ozturk, 2005).

Nowadays, concrete is the most preferred building material because of its high stress capacity It has recently been accepted that impact resistance is just as important as compressive strength in concrete and reinforced concrete structures. In developing countries, many structures, such as nuclear power plants, military structures, airports, railways, bridges and tunnels, are being built to more stringent lifecycle standards. Since these structures are exposed to impact effects during their lifetime, the impact resistance must be high in order not to cause any safety problems (Topcu and Guncan, 1995; Soe et al., 2013; Wan et al., 2016).

There are three types of factors that affect the concrete's impact resistance: the properties of the materials forming the concrete (aggregate type, maximum aggregate size and the water/cement ratio), the properties of the additives (mineral type and the proportions used in the mixture, the geometry, the slenderness of the fiber and the proportions used in the mixture) and the environmental conditions (concrete temperature and loading rate) (Oltulu and Altun, 2018).

One of the most effective methods to improve the mechanical properties and impact resistance of concrete is

* *Corresponding author*. Tel.: +90-442-231-4615 ; Fax: +90-442-231-4910 ; E-mail address: mroltulu@atauni.edu.tr (M. Oltulu)
ISSN: 2149-8024 / DOI: https://doi.org/10.20528/cjsmec.2019.01.003

to add fibers. Studies in published literature report two main reasons for this improved performance when fiber is added: 1) the fiber absorbs impact energy, and 2) it prevents disaggregation by functioning as a bridge between cracks.

Different fiber types are employed in concrete production. These include steel fiber, polypropylene fiber, glass fiber, basalt fiber, polyamide fiber, polyvinyl alcohol fiber, ceramic fiber, polyethylene fiber, nylon fiber, kevlar fiber and natural fiber. Among these, the ones most frequently used are steel and polypropylene fiber, and as can be seen from Table 1, the steel fiber has the greatest effect on the impact resistance of concrete. Besides the choice of fiber type in the mixture, the geometry, slenderness ratio and fiber fraction also affect the impact resistance of the concrete. The studies in the literature illustrating these impacts are discussed below shortly. The ratio of fiber over concrete volume is presented as a percentage.

Table 1. An overview of existing studies on fiber-reinforced concrete under impact test.

Researcher(s), (Year)	Fiber type and volume ratio (%)	Other variables	Variation vs. control specimen (%)
Swamy and Jojagha (1982)	Steel fiber (SF) (1.0)	Fiber geometry	%520 - 3505
Mindess et al. (1986)	Polypropylene fiber (PF) (0.5)	Water/cement ratio	%19 -24
Mindess and Vondran (1988)	PF (0.1-0.3-0.5)		%12-40
Mindess and Yan (1993)	PF (1.0), SF (1.0)	Loading rate	%(-22)-86
Wang et al. (1996)	PF (0.25-0.5) SF (0.25-0.5-0.75-1.0)		%17-582
Toutanji et al. (1998)	PF (0.1-0.3-0.5)	Silica fume ratio, fiber length	%40 -4100
Banthia et al. (1998)	Carbon fiber (1.0) macro and micro SF (1.0)		%3.6 -210
Nataraja et al. (1999)	SF (0.5)		%80
Marar et al. (2001)	SF (0.5-1.0-1.5-2.0)	Aspect ratio	%260-7360
Song et al. (2005)	SF (1.0)		%317
Nataraja et al. (2005)	SF (0.5-1.0-1.5)	Water/cement ratio	%268 - 2450
Ramakrishna and Sundararajan (2005)	Natural fiber (0.5-1.0-1.5-2.0)		%40 -1713
Badr et al. (2005)	PF (0.7)		%40
Yazıcı and Sezer (2008)	SF (1.0)	Maximum aggregate size	%682-800
Zeynal (2008)	Micro SF (0.3) SF (0.4-0.8-1.2)	Water/cement ratio	%210-4095
Mohammadi et al. (2009)	SF (1.0-1.5-2.0)		%41-67
Xu et al. (2010)	PVA fiber (0.3-0.6-0.9-1.2)		%23-91
Nili and Afroughsabet (2010a)	SF (0.5-1.0)	Water/binder ratio	%232-2516
Nili and Afroughsabet (2010b)	PF (0.2-0.3-0.5)	Water/cement ratio	%42- 845
Erdem et al. (2011)	SF(1.0) , PF (1.0)		%(-57)-414
Caf (2012)	SF(0.5-1.0-1.5-2.0) PF (gr) 300-600-900-1200		%1-1064
Nia et al. (2012)	PF (0.2-0.3-0.5) SF (0.5-1.0)	Water/binder ratio	%42-2516
Su and Xu (2013)	Ceramic fiber (0.1-0.2-0.3)		%(-28)-47
Aliabdo et al. (2013)	PF(0.1-0.2) SF (1.0-2.0)	Agregate type	%13-81
Gupta et al. (2015)	Rubber fiber (5-10-15-20-25)	Water/binder ratio, Silica fume ratio	%46-472

Swamy and Jojagha (1982) reported that hooked and paddle-shaped fibers gave the best results against impact loads due to their longer lengths and higher slenderness ratios. Additionally, Marar et al. (2001) and Mohammedi et al. (2009) illustrated that with increasing fiber slenderness ratio and mixing proportions, there was an increase in the concrete's impact resistance.

This study aimed to investigate the optimum rate of reuse of RCAs in concrete, and to determine the influence on the mechanical properties of RACs when used with

polypropylene and steel fibers separately and in combination (hybrid), because there is a limited number of studies about the use of hybrid fibers. Although the impact strength of concrete with hybrid fibers and with RAC was separately investigated, the impact strength of RAC with hybrid fibers was not considered. For this purpose, all concrete specimens were prepared with a water/binder ratio of 0.50, 5% silica fume and aggregates with a maximum size of 16 mm. The RCAs were used at proportions of 30% and 50% in place of the natural aggregates. Hooked-end steel fibers at a volume fractions of 1% and 2%, and polypropylene fibers at a volume fraction of 0.1%, were used separately and in combination. The mechanical properties (compressive strength, flexural strength and impact resistance) of all concrete specimens were assessed and compared to the control groups.

Using hybrid fibers in both NCs and RACs assured better performance under compressive and flexural strength tests. The hybridization of steel fiber and polypropylene fiber could enhance the mechanical properties of concrete by bridging macro-crack and delaying micro-cracks.

2. Experimental Program

2.1. Materials

In this study, Type 1 42.5 R Portland cement and silica fume (SF) were used as the cementitious materials, and their chemical compositions are summarized in Table 2. The specific gravity of Portland cement and silica fume are 3.14 and 2.24, respectively.

Table 2. Chemical components of cement and silica fume.

	Cement (%)	Silica Fume (%)
SiO_2	18.73	91.92
Al_2O_3	4.56	0.42
Fe_2O_3	3.07	0.20
CaO	63.91	2.06
MgO	2.08	3.69
SO_3	2.90	-
K_2O	0.62	-
Na_2O	0.29	-
Cl	0.02	-
Cr_2O_3	-	0.37
C	-	0.21
S	-	0.07

Both natural crushed limestone aggregates and RCAs with a maximum particle size of 16 mm were used as a coarse aggregate. Local river sand was used as a fine aggregate (NFA). The specific gravity and water absorption capacity of the aggregates were determined according to the EN 1097-6 Standard. The experiments conducted on the aggregate showed that the RCAs are about 16% weaker than the NCAs (natural coarse aggregates) because of their high porosity, and also that the water absorption of the RCAs is almost 3 times higher than that of the NCAs. Similar results were seen in published literature (Topçu and Şengel, 2004; Rao et al., 2007; Tam et al., 2008; Matias et al., 2013; Wagih et al., 2013). The physical properties of all aggregates are given in Table 3.

Table 3. Physical properties of natural aggregates and recycled coarse aggregates.

	Specific gravity	Water absorption (%)	Surface moisture (%)	Bulk density (g/cm3)
0-2 NFA	2.45	2.09	0.20	2.40
2-4 NFA	2.45	2.39	0.30	2.39
4-8 NCA	2.54	1.51	0.25	2.50
4-8 RCA	2.12	6.64	4.21	1.96
8-16 NCA	2.64	1.95	0.45	2.59
8-16 RCA	2.24	8.19	5.47	2.10

Polypropylene fibers of 9 mm in length and steel fibers of 35 mm in length with a 65 aspect ratio were used both separately and in combination. The pictures of the fibers are shown in Fig. 1, and the physical and mechanical properties of polypropylene and steel fibers are presented in Table 4.

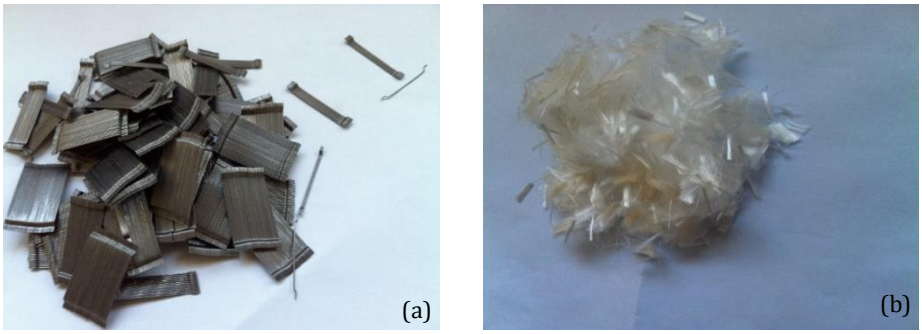

Fig. 1. (a) Polypropylene fibers; (b) steel fibers used for reinforced concrete.

Table 4. The physical and mechanical properties of polypropylene fibers and steel fibers.

	Length (mm)	Diameter (mm)	Density (gr/cm³)	Tensile strength (N/mm²)	Modulus of elasticity (kN/mm²)
Polypropylene Fiber	9	0.022	0.90	600 - 750	3.8
Steel Fiber	35	0.55	7.80	1338 - 1352	210

2.2. Mixing proportions

A cement content of 350 kg/m³ and the same water-binder ratio (W/C+SF) of 0.50 were used in all batches. To improve the mechanical properties, silica fume was used at 5% of cement weight in all concrete specimens. Super plasticizer (SP)-based polycarboxylic ether was used at 2% of cement weight in all batches for better workability.

Hooked-end steel fibers at 1% and 2% volume fractions, and polypropylene fibers at a 0.1% volume fraction were used. The NCAs used in the production of NC were replaced with RCAs 30% and 50%. The mixing proportions are listed in Table 5.

Table 5. Concrete mix proportions for 1 m³.

	W/(C+SF)	Water (kg/m³)	Cement (kg/m³)	Silica fume (kg/m³)	8-16 mm (kg/m³)		4-8 mm (kg/m³)		2-4 mm NFA (kg/m³)	0-2 mm NFA (kg/m³)	PF V_f (%)	SF V_f (%)
					NCA	RCA	NCA	RCA				
N	0.50	175	333	17	687	-	283	-	244	531	-	-
NP	0.50	175	333	17	687	-	283	-	244	531	0.1	-
NS1	0.50	175	333	17	687	-	283	-	244	531	-	1
NS2	0.50	175	333	17	687	-	283	-	244	531	-	2
NPS1	0.50	175	333	17	687	-	283	-	244	531	0.1	1
NPS2	0.50	175	333	17	687	-	283	-	244	531	0.1	2
R30	0.50	175	333	17	481	175	198	71	244	531	-	-
R30P	0.50	175	333	17	481	175	198	71	244	531	0.1	-
R30S1	0.50	175	333	17	481	175	198	71	244	531	-	1
R30S2	0.50	175	333	17	481	175	198	71	244	531	-	2
R30PS1	0.50	175	333	17	481	175	198	71	244	531	0.1	1
R30PS2	0.50	175	333	17	481	175	198	71	244	531	0.1	2
R50	0.50	175	333	17	343	291	142	118	244	531	-	-
R50P	0.50	175	333	17	343	291	142	118	244	531	0.1	-
R50S1	0.50	175	333	17	343	291	142	118	244	531	-	1
R50S2	0.50	175	333	17	343	291	142	118	244	531	-	2
R50PS1	0.50	175	333	17	343	291	142	118	244	531	0.1	1
R50PS2	0.50	175	333	17	343	291	142	118	244	531	0.1	2

Different codes have been used to identify the individual concrete groups to make the results easier to understand and interpret. The abbreviations are normal concrete (N), recycled aggregate concrete (R), polypropylene fiber (P), 1% steel fiber (S1) and 2% steel fiber (S2).

2.3. Mixing procedure

All materials were mixed in a pan mixer. Firstly, the dry coarse and fine aggregates were mixed together for one minute in the mixer. Then cement and silica fume were added and mixed for another minute. Later, water equivalent to 70% of the water required for the mix was added. Then, a hyper plasticizer was mixed with the rest of the required water, and they were added to mix with the cementitious composite for another 2 minutes. In fibrous samples, the fibers were added last and mixed together with the mixture for another two minutes. The total mixing time in non-fiber samples was five minutes, while in fibrous samples it was six minutes.

2.4. Test methods

All specimens were stored in molds for about 24 hours and were then cured in lime-saturated water at a

temperature of 23 ± 2°C, until the day of testing. Each value was determined by calculating the average of 3 different specimens. Compressive strength tests were performed at 28 days on 150x150x150 mm cubic specimens, and the flexural strength test was also performed at 28 days on 70x70x280 mm beam specimens. The compressive strength and flexural strength of specimens were determined in accordance with EN 12390-3 and EN 12390-5 Standarts, respectively.

The impact tests were conducted with the drop weight test machine as described at ACI Commitee 544, is shown in Fig. 2. The aparatus of the equipment are hammer, steel bowl and the test specimen. In this method briefly, 4.45 kg hammer is dropped sequentially from heights of up to 457 mm on the steel bowl with 64 mm diameter which placed on the concrete disc specimen 150 mm diameter by 64 mm thick. Then number of blows about first visible crack and ultimate crack were determined.

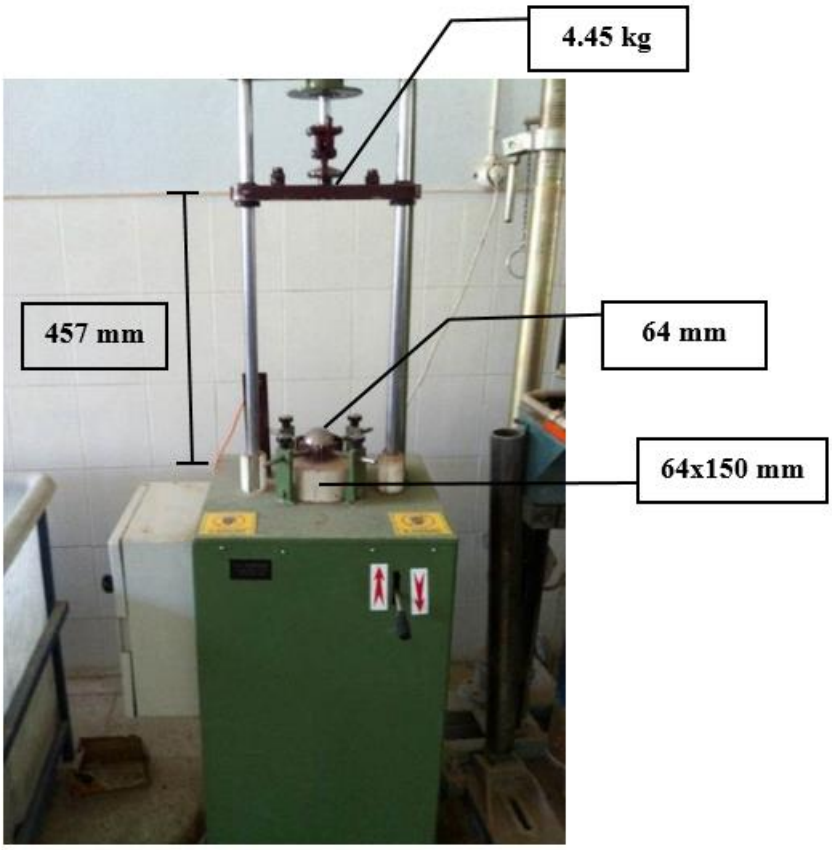

Fig. 2. Impact test machine.

The impact energy can be calculated with equations as follows:

$$H = gt^2/2 \quad (1)$$

$$V = gt \quad (2)$$

$$m = W/g \quad (3)$$

$$U = mV^2/2 \quad (4)$$

$$Impact\ energy = n \cdot U \quad (5)$$

U = Energy occured with a blow (kNmm),
W = Weight of hammer (kg),
m = Mass of hammer (N),
H = Drop height of hammer (mm),
t = Drop time of hammer (s),
g = Acceleration of gravity (mm/s^2),
V = Velocity of hammer at the moment of blow (mm/s),
n = Number of blows.

3. Results and Discussion

3.1. Compressive and flexural strengths

The compressive and flexural tests were performed on NCs, RACs, fiber-reinforced concretes and fiber-reinforced RACs. The results of compressive and flexural tests are shown in Table 6 and Fig. 3.

It was found that in R30 and R50 concrete groups, the 28-day compressive strengths were lower than that of the control group by 7% and 24%, respectively. The reason due to the second RA-cement paste interface in addition to the interface of the aggregate-cement paste (Evangelista and Brito, 2007; Hoffman et al., 2012; Butler et al., 2013; Lima et al., 2013). For that reason the RAs can be used at a 30% ratio instead of normal aggregates in concretes, and they should not exceed that ratio.

It was found that the 28-day compressive strengths of R30S1 concrete groups were higher than the control groups by 1%. In the R30S1 groups, the negative effect of RA was countered why the steel fibers. A polypropylene

and steel fiber mixture in a 1% ratio positively affected the 28-day compressive strength in both NCs and RACs. The NPS1 concrete group showed the maximum performance with a 21% increase in compressive strength compared to the control group (N), while R30PS1 had a 3% increase compared to the control group (N).

Table 6. The results of compressive and flexural tests.

	Compressive strength (MPa)	Increase/decrease compared to NC (%)	Flexural strength (MPa)	Increase/decrease compared to NC (%)
N	38.6	---	5.24	---
NP	40.9	6	5.49	5
NS1	44.5	15	7.02	34
NS2	28.8	-25	7.83	49
NPS1	46.7	21	7.51	43
NPS2	29.8	-23	7.98	52
R30	36.0	-7	4.79	-9
R30P	37.2	-4	4.93	-6
R30S1	39.0	1	6.07	16
R30S2	28.8	-25	7.05	35
R30PS1	39.6	3	6.18	18
R30PS2	29.3	-24	7.32	40
R50	29.2	-24	4.00	-24
R50P	29.9	-23	4.10	-22
R50S1	30.8	-20	5.29	1
R50S2	26.5	-31	6.81	30
R50PS1	31.6	-18	5.33	2
R50PS2	27.9	-28	6.85	31

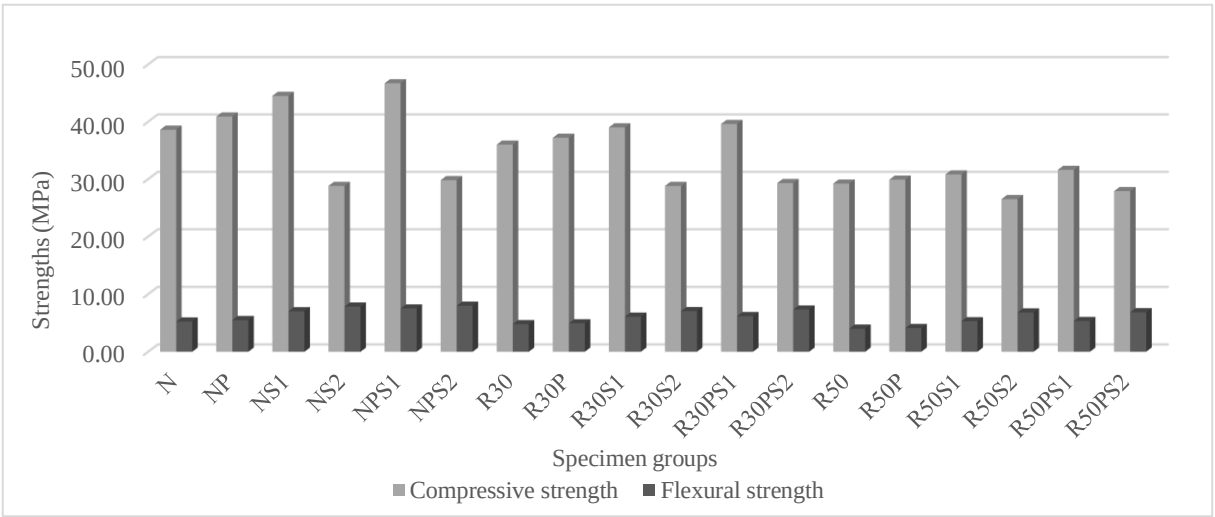

Fig. 3. Test results of compressive and flexural strengths.

The flexural strengths increased with the increase in steel fiber content. The amount of increase in the flexural strength in this study was 34% and 49% in 1% and 2% steel fiber-reinforced concretes, respectively. Fibers incorporated into concrete can hamper the growth of the cracks inside the concrete and improve the tensile strength and ductility of the concrete (Chenkui and Guafon, 1995; Eren and Celik, 1997; Abdul-Ahad and Aziz, 1999; Pajak and Ponikiewski, 2013; Khaloo et al., 2014).

In addition, 30% RACs, and 1% and 2% of steel fibers increased the flexural strength by 16% and 35%, respectively. Furthermore, adding 50% RACs, and 1% and 2% of steel fibers increased the flexural strength by 1% and 30%, respectively. According to these results, the addition of fiber gives more positive results in RACs. In this study the rates of increase were 18%, 40%, 2% and 31% for the R30PS1, R30PS2, R50PS1 and R50PS2 groups, respectively.

Using hybrid fiber in both NCs and RACs improved the performance of flexural strength and compressive strength in the specimens. The flexural strength of NPS1 and NPS2 specimens were 43% and 52% higher than the N concrete specimens. The increase in flexural strength is mainly due to the bridging effect of fibres, which restrains crack formation. Compared to the N concrete group, the flexural strength of the R30PS1 and R30PS2 concrete groups were higher by 18% and 40%, respectively. Also, compared to the N concrete group, the flexural strength of the R50PS1 and R50PS2 concrete groups were higher by 2% and 31%, respectively. According to the experimental results, the flexural strength of the hybrid fiber-reinforced concrete groups showed the best performance. The mechanical properties of RAC improved with the hybrid fiber content. This result implies that hybrid fibers should be used, especially in the RAC, depending on the fiber type and the amount.

3.2. Impact resistance

The results of impact tests, performed on recycled aggregate concretes, steel fiber concretes, polypropylene fiber concretes and hybrid fiber concretes, are presented in Table 7 and shown in Fig. 4.

Table 7. The results of impact test.

	First crack (blows)	First crack impact energy (kNmm)	Failure crack (blows)	Failure crack impact energy (kNmm)
N	142	2889	145	2950
NP	146	2963	151	3071
NS1	617	12553	1140	23498
NS2	1004	20426	1967	40019
NPS1	676	13753	1155	23498
NPS2	1057	21505	1994	40568
R30	131	2665	132	2686
R30P	142	2889	149	3031
R30S1	517	10518	889	18087
R30S2	788	16032	1321	26876
R30PS1	536	10905	899	18290
R30PS2	797	16215	1342	27303
R50	68	1383	69	1404
R50P	74	1506	79	1607
R50S1	386	7853	675	13733
R50S2	487	9908	1017	20699
R50PS1	394	8016	688	13997
R50PS2	498	10132	1031	20976

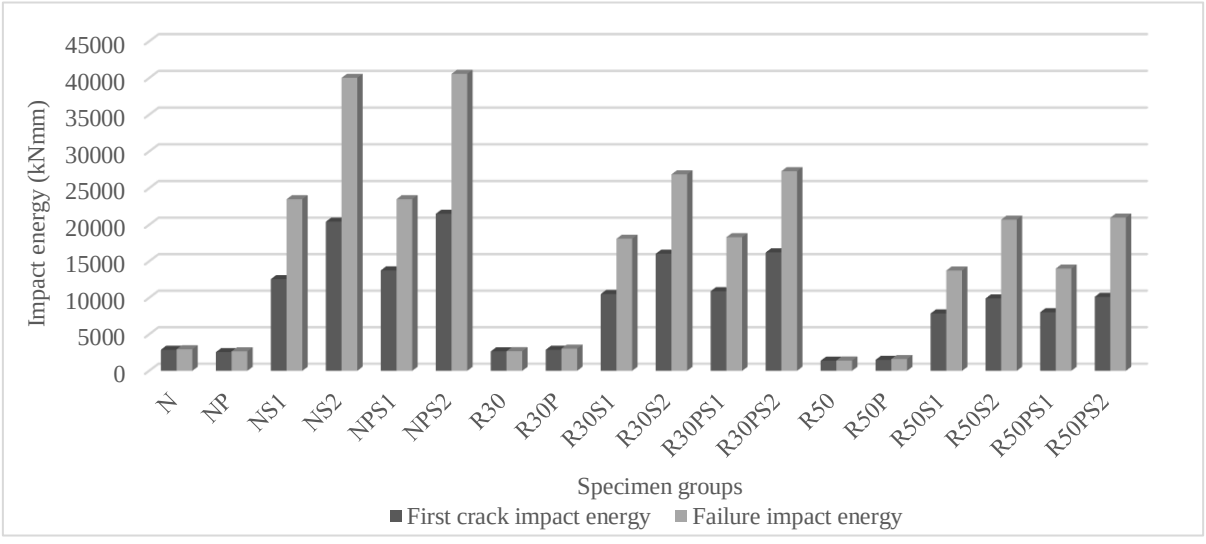

Fig. 4. Test results of impact resistance.

According to the values illustrated in Table 7, the energy at the first visible crack, and the failure energy of the R30 sample, were both lower than the control group at 8%. Also in the R50 sample, both the energy at the first visible crack and the failure energy were lower than the control group at 52% ratio. It appeared that the use of RCAs adversely affected the impact resistance of the concretes. The impact energy of concretes decreased with the increased proportion of RCA, likewise with the results for the compressive and flexural strength tests. The reason for this is the adherence between the cement paste and the RAs is weaker than the adherence between the cement paste and the natural aggregate (Erdem et al., 2011; Medina et al., 2014).

Using of 0.1% polypropylene fiber slightly increased the impact resistance in both NCs and RACs as confirmed by Badr et al. (2005), Nili and Afroughsabet (2010b), Mindess et al. (1986), Mindess and Vondran (1988), Mindess and Yan (1993), Wang et al. (1996), Toutanji et al. (1998) about the results of normal concretes.

Steel fibers increased the impact resistance of concretes too much due to their high energy absorption capacity, and the impact resistance increased with an increase in the steel fiber volume fraction (Marar et al., 2001; Mindess and Yan, 1993; Wang et al., 1996; Nataraja et al., 1999; Song et al., 2004; Nataraja et al., 2005; Mohammadi et al., 2009). In this study using 1% steel fiber increased the first crack energy and failure energy 4.5 times and 8.0 times respectively. As well as use of 2% steel fiber increased the first crack energy and failure energy 7.0 times and 13.5 times respectively.

Using steel fibers increased the impact resistance of RACs as it did for NCs. The use of 1% steel fiber in RACs with 30% RCA content increased the first crack energy and failure energy 3.5 times and 6.0 times, respectively. RACs with 50% RCA content and 1% steel fiber increased the first crack energy and failure energy about 3 times and 4.5 times respectively. RACs with 30% RCA content and 2% steel fiber increased the first crack energy and failure energy 5.5 times and 9 times, respectively, and 2% steel fiber in RACs with 50% RCA content increased the first crack energy and failure energy 3 times and 7 times respectively.

The compressive and flexural tests showed that hybrid fibers contributed to better impact resistance compared to other concrete groups. Compared to the NC, the impact resistance of NPS1, NPS2, R30PS1, R30PS2, R50PS1 and R50PS2 concrete groups were 5 to 8 times, 7 to 14 times, 4 to 6 times, 6 to 9 times, 3 to 5 times and 3.5 to 7 times higher, respectively. This result indicates that the mixed fibers have an important role in increasing the impact strength and should be taken into consideration in future work.

Using RCA decreased both the flexural strength and impact resistance, whereas using polypropylene fiber, steel fiber and hybrid fiber increased both the flexural strength and the impact resistance. The relationship between impact energy and flexural strength is shown in Fig. 5. It is understood from the correlation coefficient in the figure that there is a relationship between flexural strength and impact resistance.

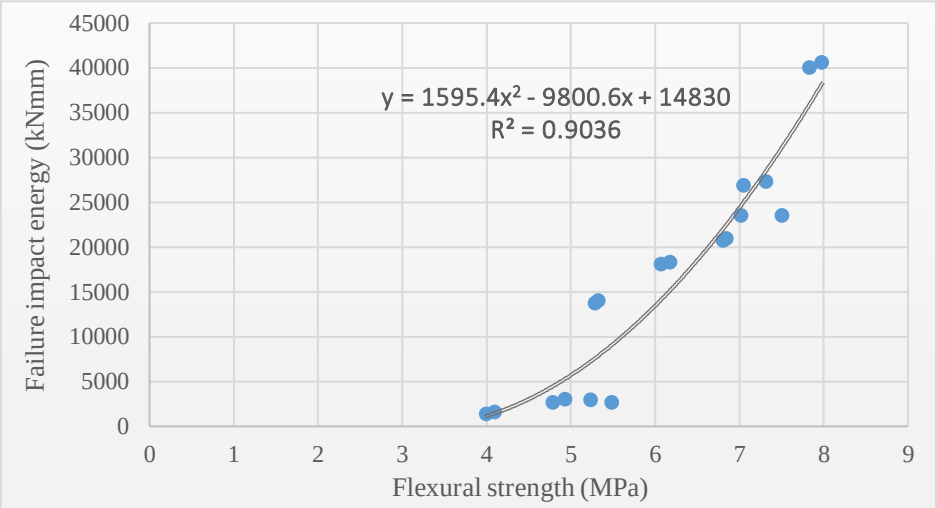

Fig. 5. Relationship between flexural strength and failure impact energy.

4. Conclusions

The main conclusions obtained from this study are as follows;

- The results of the compressive, flexural and impact tests showed that the use of RCA decreased the compressive strength, flexural strength and impact resistance of concrete. The addition up to 30% of RCA did not result in a significant difference between RAC and NC. These results have shown that up to 30% coarse RCA can be used without having any detrimental impact.
- In both NCs and RACs, using polypropylene fiber increased compressive strength and flexural strength by a small amount. While using steel fiber and hybrid fiber at a volume fraction of 1.0% increased the compressive strength, flexural strength and impact resistance, using a volume fraction of 2.0% just reduced the compressive strength because of its poor workability. By contrast, using steel fiber and hybrid fiber at 2.0% showed the best results.
- Polypropylene fibers made no significant contribution to impact resistance for any of the concrete

groups. Steel fibers increased the impact resistance of concretes too much due to their high energy absorption capacity. Hybrid fibers play an important role in increasing the impact strength and should be taken into consideration in future work on the effects on flexural strength and impact resistance.

- Considering environmental and economic impacts, it is expected that the use of RA will become more widespread and its contributions to the national economy will be increased. In addition, with these studies, it is considered that the number of facilities for the aggregate recovery and concrete recycling will increase throughout the country and thus there will be great progress in waste evaluation.
- Although many scientific studies were carried out about RACs, but there are no enough research about hybrid fiber reinforced recycled aggregate concretes. For future work, the various mechanical and durability properties of RACs should be investigated with using hybrid fibers at different ratios and using different parameters. Especially comparing studies about to different impact test methods should be examined. In addition, workability of fresh concrete, the compatibility of recycled aggregate-cement-plasticizer, should be investigated with the help of SEM, MIP analyses, XRD patterns.

REFERENCES

Abdul-Ahad RB, Aziz QQ (1999). Flexural strength of reinforced concrete t-beams with steel fibers. *Cement and Concrete Composites,* 21, 263-268.

ACI Commitee 544 (1999). ACI 544. Measurement of properties of fiber reinforced concrete. USA.

Aliabdo AA, Abd-Elmoaty AM, Hamdy M (2013). Effect of ınternal short fibers, steel reinforcement and surface layer on impact and penetration resistance of concrete. *Alexandria Engineering Journal,* 52, 407-417.

Badr A, Ashour AF, Platten AK (2005). Statistical variations in impcat resistance of polypropylene fibre reinforced concrete. *International Journal of Impact Engineering,* 32, 1907-1920.

Banthia N, Yan C, Sakai K (1998). Impact resistance of fiber reinforced concrete at subnormal temperatures. *Cement and Concrete Composites,* 20, 393-404.

Butler L, West JS, Tighe SL (2013). Effect of recycled concrete coarse aggregate from multiple sources on the hardened properites of concrete with equivalent compressive strength. *Construction and Building Materials,* 47, 1292-1301.

Caf M (2012). Impact strenght of steel and polyproplene fiber reinforced concrete. *MSc thesis*, Atatürk University, Erzurum.

Chenkui H, Guafon Z (1995). Properties of steel fibre reinforced concrete containing larger coarse aggregate. *Cement and Concrete Composites,* 17, 199-206.

EN 12390-3/AC (2012). Testing hardened concrete - Part 3: Compressive strength of test specimens,

EN 12390-5 (2010). Testing hardened concrete - Part 5: Flexural strength of test specimens.

Erdem S, Dawson AR, Thom NH (2011). Microstructure linked strength properties and impact response of conventional and recycled concrete reinforced with steel and synthetic macro fibers. *Construction and Building Materials,* 25, 4025-4036.

Eren O, Celik T (1997). Effect of silica fume and steel fibers on some properties of high strength concrete. *Construction and Building Materials,* 11, 373-382.

Evangelista L, Brito JD (2007). Mechanical behaviour of concrete made with fine recycled concrete aggregates. *Cement and Concrete Composites,* 29, 397-401.

Gupta T, Sharma RK, Chaudhary S (2015). Impact resistance of concrete containing waste rubber fiber and silica fume. *International Journal of Impact Engineering,* 83, 76-87.

Hoffmann C, Schubert S, Leemann A, Motavalli M (2012). Recycled concrete and mixed rubble as aggregates: influence of variations in composition on the concrete properties and their use as structural material. *Construction and Building Materials,* 35, 701-709.

Khalaf FM, Devenny AS (2004). Recycling of demolished masonary rubble as coarse aggregate in concrete: review. *ASCE Journal of Meterials in Civil Engineering,* 16, 331-340.

Khaloo A, Raisi EM, Hosseini P, Tahsiri H (2014). Mechanical performance of self compacting concrete reinforced with steel fibers. Construction and Building Materials, 51, 179-186.

Lima C, Caggiano A, Faella C, Martinelli E, Pepe M, Realfonzo R (2013). Physical properties and mechanical behaviour of concrete made with recycled aggregates and fly ash. *Construction and Building Materials,* 47, 547-559.

Marar K, Eren O, Celik T (2001). Relationship between impact energy and compression toughness energy of high-strength fiber-reinforced concrete. *Materials Letters,* 47, 297-304.

Matias D, Brito JD, Rosa A, Pedro D (2013). Mechanical properties of concrete produced with recycled coarse aggregates - influence of the use of superplasticizers. *Construction and Building Materials,* 44, 101-109.

Medina C, Rojas MISD, Frias M (2013). Freeze-thaw durability properties of concrete using contaminated ceramic aggregate. *Journal of Cleaner Production,* 40, 151-160.

Mindess S, Banthia N, Bentur A (1986). The response of reinforced concrete beams with a fibre concrete matrix to impact loading. *The International Journal of Cement Composites and Lightweight Concrete,* 8, 165-170.

Mindess S, Vondran G (1988). Properties of concrete reinforced with fibrillated polypropylene fibres under impact loading. *Cement and Concrete Research,* 18, 109-115.

Mindess S, Yan C (1993). Perforation of plain and fibre reinforced concretes subjected to low velocity impact loading. *Cement and Concrete Research,* 23, 83-92.

Mohammadi Y, Azad RC, Singh SP, Kaushik SK (2009). Impact resistance of steel fibrous concrete containing fibres of mixed aspect ratio. *Construction and Building Materials,* 23, 183-189.

Nataraja MC, Dhang N, Gupta AP (1999). Statistical variations in impact resistance of steel fiber reinforced concrete subjected to drop weight test. *Cement and Concrete Research,* 29, 989-995.

Nataraja MC, Nagaraj TS, Basavaraja SB (2005). Reproportioning of steel fibre reinforced concrete mixes and their impact resistance. *Cement and Concrete Research,* 35, 2350-2359.

Nia AA, Hedeyatian M, Nili M, Afroughsabet V (2012). An experimental and numerical study on how steel and polypropylene fibers affect the impact resistance in fiber reinforced concrete, *International Journal of Impact Engineering,* 46, 62-73.

Nili M, Afroughsabet V (2010a). Combined effect of silica fume and steel fibers on the impact resistance and mechanical properties of concrete. *International Journal of Impact Engineering,* 37, 879-886.

Nili M, Afroughsabet V (2010b). The effects of silica fume and polypropylene fibers on the impact resistance and mechanical properties of concrete. *Construction and Building Materials,* 24, 927-933.

Oikonomou ND (2005). Recycled concrete aggregates. *Cement and Concrete Composites,* 27, 315-318.

Oltulu M, Altun MG (2018). The drop weight test method to determine impact strength of concrete and a review of research, *Gümüşhane University Journal of Science and Technology,* 8, 155-163.

Ozturk M (2005). Construction Waste Management. Ankara.

Pajak M, Ponikiewski T (2013). Flexural behaviour of self compacting concrete reinforced with different types of steel fibers. *Construction and Building Materials,* 47, 397-408.

Ramakrishna G, Sundararajan T (2005). Impact strenght of a few natural fibre reinforced cement mortar slabs: a comparative study. *Cement and Concrete Composites,* 27, 547-553.

Rao A, Jha KN, Misra S (2007). Use of aggregates from recycled conctruction and demolition waste in concrete. *Resources Conservation and Recycling,* 50, 71-81.

Soe KT, Zhang YX, Zhang LC, (2013). Impact resistance of hybrid-fiber engineered cementitious composite panels. *Composite Structures*, 104, 320-330.

Song PS, Hwang S (2004). Mechanical properties of high strength steel fiber reinforced concrete. *Construction and Building Materials,* 18, 669-673.

Song PS, Hwang S, Sheu BC (2005). Strength properties of nylon and polypropylene fiber reinforced concretes. *Cement and Concrete Research,* 35, 1546-1550.

Su H, Xu J (2013). Dynamic compressive behavior of ceramic fiber reinforced concrete under impact load. *Construction and Building Materials,* 45, 306-313.

Swamy RN, Jojagha AH (1982). Impact resistance of steel fibre reinforced lightweight concrete. *The International Journal of Cement Composites and Lightweight Concrete*, 4, 209- 220.

Tam VWY, Wang K, Tam CM (2008). Assessing relationships among properties of demolished concrete, recycled aggregate and recycled aggregate concrete using regression analysis. *Journal of Hazardous Meterials,* 152, 703-714.

Topcu IB, Guncan NF (1995). Using waste concrete as aggregate. *Cement and Concrete Research,* 25, 1385-1390.

Topcu IB, Sengel S (2004). Properties of concretes produced with waste concrete aggregate. *Cement and Concrete Research,* 34, 1307-1312.

Toutanji H, McNeil S, Bayasi Z (1998). Chloride permeability and impact resistance of polypropylene fiber reinforced silica fume concrete. *Cement and Concrete Research,* 28, 961-968.

Wagih AM, El-Karmoty HZ, Ebid M, Okba SH (2013). Recycled construction and demolition concrete waste as aggregate for structural concrete. *Housing and Building National Research Center Journal,* 9, 193-200.

Wan F, Jiang Z, Tan Q, Cao Y (2016). Response of steel tube confined concrete targets to projectile impact. *International Journal of Impact Engineering,* 94, 50-59.

Wang N, Mindess S, Ko K (1996). Fibre reinforced concrete beams under impact loading. *Cement and Concrete Research,* 26, 363-376.

Xu B, Toutanji HA, Gilbert J (2010). Impact resistance of polyvinyl alcohol fiber reinforced high performance organic aggregate cementitious material. *Cement and Concrete Research,* 40, 347-351.

Yazıcı S, Sezer GI (2008). The effect of aggregate maximum size on impact resistance of fiber reinforced concrete. *Pamukkale University Journal of Engineering Sciences,* 14, 237-245.

Zeynal E (2008). Effect of water/cement ratio and fiber content on mechanical properties and impact resistance of steel fiber reinforced concrete mixtures. *MSc thesis*, Ege University, Izmir.

Challenge Journal of Structural Mechanics

Research Article

Research on effect of the quantity and aspect ratio of steel fibers on compressive and flexural strength of SIFCON

Nurullah Soylu *, Ahmet Ferhat Bingöl

Department of Civil Engineering, Atatürk University, 25240 Erzurum, Turkey

ABSTRACT

SIFCON (Slurry Infiltrated Fiber Reinforced Concrete) is a composite which occur hardening of the matrix phase, consists of cement, water, mineral additives, fine sand, water reducing plasticizer, and reinforced with high volume fiber (5–20%). The main difference from the high strength concrete (HSC) is the ductile behaviour at failure. However, the brittleness increases with the strength increase in HSC, SIFCON has a ductile behaviour because of the high volume fiber content, low permeability, high durability. Despite fiber content is 2-3% in fiber reinforced concrete, fiber content may be ten times more in SIFCON and ductility is gained. This concrete is suggested to be used in military buildings against explosion, industrial grounds, airports, and bridge feet. In this study, in order to investigate the compressive and flexural strengths of SIFCON, the aspect ratio and fiber volume of steel fibers were chosen as variable and the effects of these parameters on compressive and flexural strengths were investigated. In the study, steel fibers with aspect ratio of 40, 55, 65, and 80 were used in 0, 4, 8 and 12% ratios. The water/binder ratio was kept constant at 0.35. Silica fume is used 10% and water-reducing plasticizer is used 1.5% of cement by weight. 7 and 28 days cured samples were subjected to compressive and flexural tests and the results were compared. As a result of the tests carried out, increases in both the compressive and flexural strengths of SIFCON specimens were determined with increasing fiber volume up to 8%. Strength reductions were observed at higher ratios. In cases where the fiber volume is too high, it has been seen that the strengths were decreased. The reason of strength reduction can be explained by the difficulty of passing ability of mortar between the fibers. The highest strengths were obtained from fibers with the aspect ratio of 80. Increase in the aspect ratio as well as increases in compressive and flexural strengths have been found.

ARTICLE INFO

Article history:
Received 12 December 2018
Revised 4 February 2019
Accepted 11 February 2019

Keywords:
SIFCON
Steel fiber
Aspect ratio
Compressive strength
Flexural strength

1. Introduction

Concrete is an important building material which is obtained by mixing the aggregate (fine and coarse aggregate), water, cement and if necessary, the mineral admixtures according to the desired property and strengthening the initial plastic consistency over time.

Technical features can be developed by adding different materials to the concrete in order to improve and strengthen the weak properties of concrete (Topçu and Boğa, 2005). In order to achieve the desired performance in concrete, special concretes have been developed by producing concrete suitable for different applications. One of the special concrete types is fiber concrete. Fibers; glass, steel, plastic, different types of materials, such as aspect ratio and different sizes are produced. Such fibers are used in concretes by different volumes to improve the properties of the concrete, in particular the energy absorption capacity and flexural strength. For this purpose, mineral, metallic, polymer or natural materials having a certain ratio (size / diameter) of specificity mixed with different methods of fresh concrete are

* *Corresponding author*. Tel.: +90-442-233-1505 ; E-mail address: nsoylu@gmail.com (N. Soylu)
ISSN: 2149-8024 / DOI: https://doi.org/10.20528/cjsmec.2019.01.004

called fiber. The American Concrete Institute (ACI) committee is considered the best parameter for defining the fiber-to-fiber volume, which is the ratio of the length of the fiber to the equivalent fiber diameter. Equivalent fiber diameter; is defined as the diameter of a circle equal to the cross-sectional area of the fiber. The tensile stress and geometric structure of the fiber are the other parameters that define the fiber (Ünal et al., 2007).

SIFCON (Slurry Infiltrated Fiber Concrete) is a cement-based, high-engineering, high-density fiber-reinforced mixture of cement, superplasticizer, very fine sand and silica fume. SIFCON's high compressive strength, flexural strength and toughness make this special concrete type superior to traditional concretes. Due to these advantages of SIFCON, it is recommended to be used in building explosion-proof structures, bridge piers exposed to high deformation and/or industrial floors (Alcan and Bingöl, 2019).

The most important feature that distinguishes SIFCON from high strength concrete is that it exhibits ductile behaviour during breakage. The increase in strength is also the most important problem in high strength concrete. SIFCON, with its high durability, low permeability, strength and ductility properties, is a building material with fibers up to 20% by volume. Fiber content of fiber concretes is between 2% and 3%. In parallel with the fiber content used in SIFCON, the order of material ductility is about 10 times higher (Taşdemir and Bayramov, 2007).

SIFCON allows the use of high rates of fiber with the advantage of production technique (Arslan and Aydın, 1999). SIFCON was first produced in 1979 by the Lankard Materials Laboratory in the United States with the aim of creating a highly dense fiber system, by placing high volume of steel fibers into the mold (Lankard, 1984). The fiber matrix of SIFCON contributes significantly to the strength of concrete as similar to fibrous concrete. Since the fibers in normal fibrous concrete are mixed together with the mixing matrix, the mixing of the fibers with the matrix is limited. This limit may be 1% or 2% depending on the fiber type and workability in the mixture. The fiber volume in SIFCON can range from 5% to 30% (Lankard, 1984; Homrich and Naaman, 1987).

Fiber volume to be used in SIFCON depends on the type, length, diameter of the fiber and the vibration applied to ensure the full filling of the mixture matrix. By prolonging the vibration time, shorter fibers can be placed in a denser and higher volume than long fibers (Gilani, 2007). The fibers to be used when preparing SIFCON are randomly stacked in a desired pattern, area or plate etc. at the desired volume. The array can be made by hand to the sample mold, or by large-scale applications with machines capable of fiber distribution. As previously mentioned, the amount of fiber; fiber diameter, in particular the aspect ratio (l/d), fiber geometry and placement technique. In addition, vibration can be applied when placing the fibers. Strong vibration should be applied to achieve high fiber volumes. One of the most important factors in SIFCON manufacturing is fiber orientation. Direction is mainly perpendicular to gravity and is in two dimensions. Direction effect is more effective in some fiber types than others are. Fiber orientation is a phenomenon that should be considered when designing in laboratory or wide field applications. The preparation of SIFCON test samples should be determined based on need, avoiding uneven fiber distributions. The fiber density at the edge of the mold may be much less than inside. In addition, a number of fibers can be aligned vertically (parallel to the axis of the cylinder) along the outer surface (Lankard, 1985).

The aim of this study is to investigate the effects of fiber volume on the mechanical properties of SIFCON. Within the scope of the study, in addition to the steel fiber-free control group, 13 separate groups of SIFCON samples were produced by using 4%, 8% and 12% steel fibers in volume and with 40, 55, 65 and 80 aspect ratio.

2. Material and Methods

In this study, the Portland cement CEM II 42.5 produced by Aşkale Cement Plant was used. The physical, mechanical and chemical analysis results of this cement obtained from the producer factory are given in Tables 1 and 2.

Table 1. Physical and mechanical properties of cement.

Specific Mass (g/mL)		3.13
Litres mass (g/L)		1110
Setting time (hour)		2.10
Final set (hour)		3.15
Volume expansion. (mm)		3
Compressive strength (MPa)	2 days	23.5
	7 days	35.3
	28 days	47.0
Flexural strength (MPa)	2 days	5.0
	7 days	6.2
	28 days	7.7

Table 2. Chemical properties of cement.

Chemical Composition	Ratio (%)
SiO_2	19.94
Al_2O_3	5.28
Fe_2O_3	3.45
CaO	62.62
MgO	2.62
SO_3	2.46
Glow Loss	1.99
Na_2O	0.23
K_2O	0.83
Cl	0.0107
Unacceptable	0.08
Total	100
Free CaO	0.51
Insoluble Residue	0.70
Fe_2O_3	3.45

The MasterGlenium® ACE 450 product, produced by BASF, was used as a plasticizer additive. This product is a super plasticizing additive which increases the strength of the concrete by increasing the water content of the concrete with high amount of water with the same amount of water. 1.5% of the weight of the cement is added to the mixture. It is effective against frost and permeability. It reduces water used in the mixture by more than 20% depending on dosage. Some properties of superplasticizer additive are given in Table 3.

Table 3. Super plasticizing additive properties.

Name	BASF MasterGlenium® ACE 450
Type	Polycarboxylic Ether Based
Colour	Brown, homogeneous and liquid
Density (kg/m^3)	1 089±20
pH Value	About 5-7
Alkali Content	≤ 3.00
Chlorine Ion Content %	≤ 0.10

In this study, Silica Fume obtained from Silica Ferrochrome plant in Antalya Electrometallurgy Plant was used. The chemical composition of Silica Fume is given in Table 4. 10% of the weight of cement was used in the mixtures.

Table 4. Chemical composition of silica fume and sieve analysis.

Chemical Composition		Sieve Analysis	
Material	Amount (%)	mm	Remain (%)
Cr_2O_3		+0.250	0.3 – 1
SiO_2	85–95	+0.125	0.8 – 2.5
Fe_2O_3	0,5–1,0	+0.074	0.5 – 2.5
Al_2O_3	1.0–3.0	+0.044	1.0 – 7.5
MgO	1.0–2.0	+0.038	3.0 – 7.0
CaO	0.8–1.2	-0.038	92 – 80
C	0.5–1.0		
S	0.1–0.3		
Glow Loss	0.5–1.0		

KMX 40/30 BG, KMX 55/30 BG, KMX 65/35 BG and KMX 80/60 BG type, cold drawn steel fibers were used from Kemerli Metal Industry and Trade Joint Stock Company. The technical properties of the steel fiber used are shown in Table 5.

Table 5. Technical properties of the steel fiber.

Fiber Type	KMX 40/30 BG	KMX 55/30 BG	KMX 65/35 BG	KMX 80/60 BG
Length (mm)	30	30	35	60
Diameter (mm)	0.75	0.55	0.55	0.75
Aspect ratio (l/d)	40	55	65	80
Min. Tensile strength (N/mm^2)	1200	1500	1500	1200
Unit Quantity (fiber/kg)	9000	16750	14530	4580

In this study, natural sand is used which obtained from Erzurum Beton A.Ş. Within the scope of the study, in addition to the steel fiber-free control group, 13 separate groups of SIFCON samples were produced by using steel fibers with 40, 55, 65 and 80 aspect ratio in volume of 4%, 8% and 12%. The amount of material entering into the mixture is given in Table 6.

Compressive strengths of concretes are determined on cubic samples with 15 cm dimensions. Both 7 and 28 days strengths are calculated. Because the concrete is a material that shows deformation depending on time, the loading speed is an effective parameter on the compressive strength of the concrete (Baradan et al., 2007). Therefore, all samples were tested under a constant loading rate. For TS EN 12390-3 (2010) this value should be between 0.2 MPa/s and 1.0 MPa/s. The process of breaking the concrete samples was done by selecting the loading speed of 0.4 MPa/s.

Determination of the flexural strength of concrete according to TS EN 12390-5 (2002) and TS 10515 (1992) standards, fiber and fiberless concrete samples were made by simple beam method loaded from the midpoint of the opening in this test method. For the determination of the flexural strength, 70x70x280 mm beam samples were produced. Flexural strength is calculated using the equation given below:

$$F = 3PL/2bd^2 \quad (1)$$

where F is flexural strength (MPa), P is maximum load (N), L is clearance between abutments (mm) b and d are cross-section dimensions of the sample (mm).

The effects of fiber on compressive and flexural strength of the samples were investigated in the samples produced at different fiber volume and aspect ratios.

3. Research Results

3.1. Compressive strength test

The results of the compressive strength of SIFCON samples obtained by using fiber of different volumes and fiber of different aspect ratio with the control group for 7 days and 28 days cure application are presented in Tables 6 and 7.

Table 6. Material quantities for SIFCON (for 1 m^3 concrete).

Material / Group	Cement (kg)	Aggregate (kg)	Silica Fume (kg)	Water (kg)	Water/Binder	Plasticiser (kg)	Amount of Fiber (kg)
N0 - L0	800	950	80	308	0.35	13.2	0
N40 – L4	800	950	80	308	0.35	13.2	320
N55 – L4	800	950	80	308	0.35	13.2	320
N65 – L4	800	950	80	308	0.35	13.2	320
N80 – L4	800	950	80	308	0.35	13.2	320
N40 – L8	800	950	80	308	0.35	13.2	640
N55 – L8	800	950	80	308	0.35	13.2	640
N65 – L8	800	950	80	308	0.35	13.2	640
N80 – L8	800	950	80	308	0.35	13.2	640
N40 – L12	800	950	80	308	0.35	13.2	960
N55 – L12	800	950	80	308	0.35	13.2	960
N65 – L12	800	950	80	308	0.35	13.2	960
N80 – L12	800	950	80	308	0.35	13.2	960

Table 7. Compressive strength of 7-day samples.

Sample Code	Load (kgf)	Strength (MPa)	Percent Change by Control Sample (%)
N0 - L0 (Control Sample)	111200	48.47	0
N40 – L4	114122	49.74	2.63
N55 – L4	116691	50.86	4.94
N65 – L4	119835	52.23	7.76
N80 – L4	122200	53.26	9.89
N40 – L8	126534	55.15	13.79
N55 – L8	128943	56.20	15.96
N65 – L8	133417	58.15	19.98
N80 – L8	135872	59.22	22.19
N40 – L12	90100	39.27	-18.98
N55 – L12	95331	41.55	-14.27
N65 – L12	96478	42.05	-13.24
N80 – L12	98841	43.08	-11.12

Table 8. Compressive strength of 28-day samples.

Sample Code	Load (kgf)	Strength (MPa)	Percent Change by Control Sample (%)
N0 - L0 (Control Sample)	140415	61.20	0
N40 – L4	154525	67.35	10.05
N55 – L4	160399	69.91	14.23
N65 – L4	171136	74.59	21.88
N80 – L4	174601	76.10	24.35
N40 – L8	164689	71.78	17.29
N55 – L8	168085	73.26	19.71
N65 – L8	175404	76.45	24.92
N80 – L8	183824	80.12	30.92
N40 – L12	124630	54.32	-11.24
N55 – L12	127681	55.65	-9.07
N65 – L12	130366	56.82	-7.16
N80 – L12	134105	58.45	-4.49

3.2. Flexural strength test

The results of the 3-point flexural strength for 7-days and 28 days cure applied SIFCON samples are presented in Tables 9 and 10.

4. Conclusions

The most important outcomes of this study are listed below.

- The maximum compressive strength of 7 days cure was obtained in the N80- L8 sample group with 80 aspect ratio and 8% fiber content with 59.22 MPa. According to the control sample, an increase of 22% in compressive strength was observed.
- The maximum compressive strength of 28 days cured specimen was 80.12 MPa which is obtained from the N80-L8 group. According to the control sample, an increase in compressive strength of approximately 30% was observed.
- According to the results obtained from the experiments, it was determined that there was an increase in the compressive strength values as the aspect ratio increased.
- Increasing the fiber volume showed an increase in compressive strengths up to 8% fiber content for each aspect ratio. Over the 8% fiber volume, it became more difficult to place the matrix between the fibers, resulting in a reduction in the compressive strength.
- In the 7-day samples, the maximum flexural strength was obtained in the N80- L8 sample group with 80 aspect ratio and 8% fiber content with the value of 33.92 MPa. Flexural strength was increased by about 13 times compared to the control sample.

Table 9. Flexural strength of 7-day samples.

Sample Code	Load (kgf)	Strength (MPa)	Percent Change by Control Sample (%)
N0 - L0 (Control Sample)	284	2.44	0.00
N40 – L4	1670	14.32	487.86
N55 – L4	2163	18.55	661.51
N65 – L4	2217	19.02	680.99
N80 – L4	2482	21.29	773.94
N40 – L8	2698	23.14	849.94
N55 – L8	3125	26.80	1000.35
N65 – L8	3530	30.28	1142.96
N80 – L8	3955	33.92	1292.61
N40 – L12	2645	22.69	831.47
N55 – L12	2607	22.36	817.92
N65 – L12	3252	27.89	1045.07
N80 – L12	3580	30.71	1160.56

Table 10. Flexural strength of 28-day samples.

Sample Code	Load (kgf)	Strength (MPa)	Percent Change by Control Sample (%)
N0 - L0 (Control Sample)	402	3.45	0
N40 – L4	1888	16.19	369.53
N55 – L4	2333	20.01	480.22
N65 – L4	2656	22.78	560.66
N80 – L4	2966	25.44	637.81
N40 – L8	3380	28.99	740.80
N55 – L8	3500	30.02	770.77
N65 – L8	3669	31.47	812.56
N80 – L8	4180	35.85	939.68
N40 – L12	2824	24.22	602.43
N55 – L12	2957	25.36	635.49
N65 – L12	3422	29.35	751.21
N80 – L12	3784	32.46	841.40

- The maximum flexural strength of 28 days samples was obtained in the N80- L8 sample group with the value of 35.85 MPa. 9-fold increase in flexural strength was observed compared to the control sample. This results are similar with literaute (Farnam et al., 2010). They indicated that SIFCON's fracture energy can achieve 300-fold of fracture energy of traditional concrete while its tensile strength can achieve 7–15-fold of tensile strength of traditional concrete. These mechanical features indicate that SIFCON is a concrete with superior qualities.
- According to the results obtained from the experiments, it was found that the increase in the aspect ratio increases the flexural strength values as well as the compressive strength. However, these increases were more pronounced.
- With increasing fiber volume, increase on flexural strengths up to 8% fiber volume have been observed for each aspect ratio. After the fiber volume of 8%, it is difficult to settle between the fibers.
- As a conclusion of the experimental results, it is seen that increase on the flexural strength was more meaningful according to compressive strength for SIFCON.
- When the test results of samples with a fiber volume of 12% were examined, the aggregate used could not be infiltrated by the dense fiber network of the matrix due to the maximum diameter of 1 mm. As a result, compressive strengths decreased compared to other fiber volumes, but the flexural strengths showed decreases compared to only 8% fiber content. So it was determined that 1 mm aggregate diameter was not suitable for high fiber content.

As a conclusion of this study; the results showed that fiber addition improves the properties of concrete and high volume fiber concrete SIFCON has superior mechanical properties. Similarly, Shah and Ribakov (2011), indicated that; addition of fibers to high-strength concrete improves its mechanical properties and makes the material very attractive for applications in construction.

REFERENCES

Alcan HG, Bingöl AF (2019). Examining SIFCON's mechanical behaviors according to different fiber and matrix phase. *Iranian Journal of Science and Technology, Transactions of Civil Engineering*, (in press), 1-7.

Arslan A, Aydın AC (1999). Lifli betonların darbe etkisi altında genel özellikleri. *Çelik Tel Donatılı Betonlar Sempozyumu*, İstanbul, Turkey.

Baradan B, Yazıcı H, Ün H (2002). Betonarme Yapılarda Kalıcılık (Durabilite). Dokuz Eylül Üniversitesi Mühendislik Fakültesi Yayınları, 298, İzmir.

Farnam Y, Moosavi M, Shekarchi M, Babanajad S, Bagherzadeh A (2010). Behaviour of slurry infiltrated fibre concrete (SIFCON) under triaxial compression. *Cement and Concrete Research*, 40(11), 1571-1581

Gilani AM (2007). Various Durability Aspects of Slurry Infltrated Fiber Concrete. *Ph.D thesis*, Middle East Technical University, Ankara, Turkey.

Homrich JR, Naaman AE (1987). Stress-strain properties of SIFCON in compression. *Fiber Reinforced Concrete - Properties and Applications, ACI SP-105*, American Concrete Institute, Detroit, Michigan, 283-304.

Lankard DR (1984). Preparation, applications: slurry infiltrated fiber concrete (SIFCON). *Concrete International*, 6(12), 44-47.

Lankard DR (1985). Preparation, properties and applications of concrete - based composites containing 5% to 20% steel fiber. Steel Fiber Concrete, US-Sweden Joint Seminar, 199-217.

Shah AA, Ribakov Y (2011). Recent trends in steel fibered high-strength concrete. *Materials & Design*, 2(8), 4122-4151.

Taşdemir MA, Bayramov F (2002). Yüksek performanslı çimento esaslı kompozitlerin mekanik davranışı. *İTÜ Dergisi*, 1(2), 125-144.

Topçu İB, Boğa AR (2005). Uçucu kül ve çelik liflerin beton ve beton borularda kullanımı. *Journal of Engineering and Architecture Faculty of Eskişehir Osmangazi University*, 18(2), 1-14.

Ünal O, Uygunoğlu T, Gençel O (2007). Çelik liflerin beton basınç ve eğilme özeliklerine etkisi. *Pamukkale University Journal of Engineering Sciences*, 13(1), 23-30.